Journal of Theoretical and Applied Vibration and Acoustics 9(2) 66-102 (2023)

I S A V

Journal of Theoretical and Applied Vibration and Acoustics

journal homepage: http://tava.isav.ir

Analytical determination of Iwan and Maxwell slip models of an elastic frictional rough interface

Hossein Jamshidi *,[a], **Hamid Ahmadian** [b]

[a] *Ph.D., School of Mechanical Engineering, Iran University of Science and Technology, Tehran, Iran*

[b] *Professor, School of Mechanical Engineering, Iran University of Science and Technology, Tehran, Iran*

Research Article

ARTICLE INFO

Article history:
Received 22 September 2023

Received in revised form
10 November 2023

Accepted 5 December 2023

Available online 10 January 2024

Keywords:
Rough interface

Asperity contact

Jenkins element

Iwan model

Maxwell slip model

ABSTRACT

This paper analytically derives the Maxwell slip model associated with a frictional rough contact interface using the multi-asperity contact theory in the elastic region. The multi-asperity contact theory based on the Mindlin solution relates interface roughness, material properties, and preload to the contact interface Jenkins element parameters of the discrete Maxwell slip model and continuous Iwan model distribution function. The rough surface properties are obtained from the measured roughness profile of two contacting surfaces. The main advantage of the proposed analytical Maxwell slip model is there is no need to update or identify any parameter using experimental test data. In achieving a rough interface discrete Maxwell slip model, the interface contacting asperities are grouped based on their heights, called a height-region element group of the contact interface model. Each height-region asperities' contact area is divided into annular areas; the number of annular areas determines sliding motion states. Using the classical Mindlin solution, a Jenkins element is assigned to each specified annular area using the Hertzian normal pressure distribution function of the contact area and contribution to the tangential contact stiffness. The Iwan and Maxwell slip model's resultant hysteresis curves are compared with the analytical multi-asperity contact model to verify the proposed contact model procedure's accuracy. Model predictions of the proposed procedure are also validated against measured frictional contact behavior, resulting in good agreements with experimental observations.

Nomenclature

R	radius of spherical asperity	N	number of heights-region elements
a	radius of asperities contact area	η	combined areal density of asperities
ρ	radius of stick area of contacting asperities	A	nominal contact area of the rough interface
w	penetration depth of contacting asperities	$\Phi(z)$	probability distribution function of asperity heights
		F_{υ}	total normal force of rough interface

* Corresponding author.
E-mail address: jamshidi_hossein@alumni.iust.ac.ir (H. Jamshidi)

http://dx.doi.org/10.22064/tava.2024.2012100.1228

σ	combined standard deviations of asperity heights of the rough interface	Q_v	total tangential force of rough interface in the virgin loading phase
z	height of asperities	k_τ	tangential stiffness of two contacting asperities
y	distance between two flat rough surfaces	K_T	initial total tangential interface stiffness of the rough interface
f_υ	Hertzian normal force of two contacted asperities	$\mathrm{k}_{\tau,m}$	tangential stiffness of Jenkins element in asperity scale
f_τ	tangential friction force of two contacted asperities	$\phi_{\tau,m}$	slippage force limit of Jenkins element in asperity scale
μ	constant friction coefficient	$K_{\tau,n,m}$	tangential stiffness of equivalent Jenkins element of rough interface
x	tangential relative motion	$\phi_{\tau,n,m}$	slippage force limit of equivalent Jenkins element of rough interface
$\bar{z}_l$	slippage heights limit of asperities in the virgin loading phase	$\rho(\varphi)$	slippage distribution function of the Iwan model
$\bar{z}_{\max}$	height of the highest asperity	x_L	slippage displacement limit of rough interface
ε	relative approach of rough interface	R_q	root mean square of roughness
E, G	Young's modulus and shear moduli of contacting surface materials	R_{Pc}	peak count of measured surface profile
ν	Poisson's ratios of contacting surface materials	R_{sm}	mean value of profile elements width
S, H	shear strength and hardness (MPa)	R_{sk}	skewness of measured roughness profile
M	number of annuli	R_{ku}	kurtosis of the measured roughness profile

1. Introduction

Frictional interfaces in structural joints are among the most significant energy dissipation mechanisms that severely affect structures' dynamic behavior. These effects are due to abrupt stiffness and damping changes in the interface's normal and tangential directions. Frictional contact interface modeling is crucial for accurate prediction and controlling structural behavior. Two main approaches in modeling a frictional contact are phenomenological modeling based on matching experimental observations and physical-based modeling derived from fundamental physical principles.

In phenomenological modeling, the contact model parameters are identified by matching experimental observations of the system, and its parameters may have no physical meaning. Many phenomenological models exist in frictional contact, such as Iwan and Maxwell slip models [1-3]. The Iwan model defines contact interface restoring forces in a continuous form, while the Maxwell slip model is a discrete representation. The Iwan model defines contact interface restoring forces using an infinite number of Jenkins elements with identical stiffness and continuous distribution of critical slippage forces [4-6], which Iwan developed. Segalman later applied it to frictional interactions [1]. The various distribution functions are proposed for the critical slippage friction force of the Iwan model [5]. The Maxwell slip model consists of a finite number of parallel series of Jenkins elements. It provides a discrete representation of the contact interface behavior characterized by its Jenkins element's stiffness and critical slippage force [7]. The phenomenological discrete Maxwell slip and continuous Iwan model parameters are identified using experimental test data [8]. The development of methods to accurately identify Maxwell slip

model parameters and the slippage distribution function of the Iwan model is a challenge in practice addressed by many research studies [9-16]. Due to the widespread application of the Iwan and Maxwell slip models, this study is interested in extracting equivalent Maxwell slip model parameters and the Iwan model's slippage distribution function of two contacting rough surfaces analytically. This is done using a physical-based contact model instead of identifying them using measured test data. The physical-based multi-asperity contact model defines the interactions between contacted asperities. Its parameters depend on contacting surfaces' roughness and material properties, first presented by Greenwood [17, 18], which can be used to model the dissipated energy of contacting surfaces in vibrated structures [19].

The present study relates the phenomenological friction models to the physical-based model, which proposes an analytical procedure to determine the discrete Maxwell slip model of frictionally rough interfaces. A slippage friction force and a linear spring uniquely define each Jenkins element in the Maxwell slip model. Alternatively, a constant preload and a friction coefficient may determine the slippage friction force. The relations between stiffness and sliding force of each Jenkins element in the Maxwell slip model are obtained using multi-asperity contact theory. The modeling starts with forming the asperity heights-regions, which groups asperities with similar heights, i.e., the asperity heights' distribution function is divided into segments. An annulus element represents a height region, which defines the state of motion in regions with similar heights. The annulus elements represent the states of motion in each height region's contact area of asperities and their associated stiffness. Finally, the extracted formulations on the asperity scale are extended to the rough interface scale, using statistical summation to establish Jenkins elements of the equivalent Maxwell slip model. Using the proposed Maxwell slip model, the frictionally hysteresis behavior of the rough interface can be easily simulated by the finite number of Jenkins elements. The resultant hysteresis curves of the proposed Maxwell slip model are obtained using the determined continuous Iwan model.

The content of the current work is presented in six sections. Section 2 introduces the multi-asperity contact theory's governing equations. The elastic rough interface's equivalent Maxwell slip contact model is obtained analytically using the rough surface measured geometry in Section 3. This section compares the resultant hysteresis friction curves obtained by the introduced Maxwell slip model with the resultant curves' analytical rough interface model. It is shown that there is an excellent agreement between the analytical model and the proposed Maxwell slip model. In Section 4, the continuous Iwan model of an elastic frictional rough interface is derived using the multi-asperity contact theory. The simulation results of the proposed modeling procedure of frictionally interface, i.e., the discrete Maxwell slip and continuous Iwan model's analytical determination, are presented and compared with the experimental observations in Section 5. Finally, Section 6 draws some conclusions.

2. Multi-asperity contact theory

Greenwood [18] presented the rough surface model and defined the relation between normal contact force and penetration depth of nominally flat surfaces formulated using surface parameters. Traditional roughness measurement methods obtain the multi-asperity contact model parameters; therefore, predictions of resultant contact models depend on measuring surface roughness parameters. A unique property can be defined by measuring a rough surface profile. That is, whether a surface is repeatedly magnified, increasing roughness details are observed at all

magnifications, where the nanoscale roughness is observed besides the microscale roughness. The roughness of the surface has different heights, gradients, and peak radii, called asperities [17, 18]. The measured profile consists of asperities on asperities as a nanoscale on the microscale [20]. Greenwood explained that a single asperity in the multi-asperity contact theory is based on different scales of asperities [21]. Two common scenarios in the multi-asperity contact theory statistical method, i.e., two rough surfaces (TRS) and single rough surface (SRS) models, are visualized in Fig. **1**. Both contacting surfaces are rough in the TRS model, and the oblique contact effect of asperities is considered. In the SRS model, the contact of asperities is assumed summit to summit. The oblique contact effect in the low contact angle of asperities is considered in an SRS model by performing some modifications [22]. In the SRS model, the contact interface is simulated by a smooth, flat, rigid surface and a combined elastic rough surface. This study uses the SRS model considering the oblique contact effect on the constant friction coefficient [22].

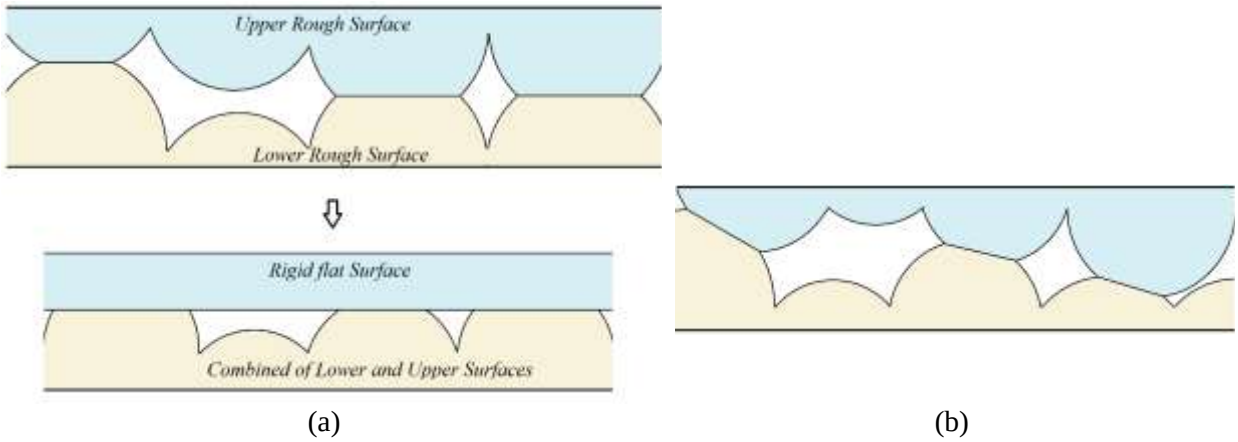

Fig. 1: Rough interface models in multi-asperity contact theory: (a) summit-to-summit contacting asperities and its equivalent SRS model, (b) oblique contact of asperities in TRS model.

In estimating shear contact between rough surfaces, the interface's state of motion is divided into pre-slip (or partial slip) and macro-slip states. Some asperities stick together in the pre-slip state, while the contact in other asperities is in the macro-slip state. On the other hand, in the sliding mode between two rough surfaces, all asperities slip. Similarly, in the asperity scale, the motion state of the whole rough interface is divided into a pre-slip and macro-slip state. In the pre-slip state, parts or whole contact areas are in stiction. In the macro-slip state, the entire contact area of asperities slips [23].

This section introduces the SRS model's governing equations, assuming the asperities summit are spherical, having the same radius, and a known height distribution function. It should be noted that the variation of summit curvature (radius) relative to asperity heights is smooth and slow [24]. Therefore, for a wide range of asperity heights, an average value can be attributed to the radius of curvature of asperities. Also, the constant normal preload is distributed uniformly on the rough interface, and the deformation of all asperities remains in the elastic range, where the deformation behavior follows Hertzian theory. The normal contact force (normal pressure) is assumed to be low and does not cause plastic deformation in asperities. Also, the assumption of elastic behavior of contacting surfaces is based on actual behavior in structures; after initial plastic deformations, vibrations of rough interfaces occur in an elastic state. Therefore, to accurately simulate the rough interface frictional behaviors in vibrating applications, the surface roughness profiles are measured

after the interfaces are exposed to vibrational loadings [18]. First, the tangential stiffness formulation of two contacting spherical asperities is derived from the stick area's radius. The SRS multi-asperity contact model defines the friction contact force-displacement and interface stiffness relations.

2.1. Contact theory of two spherical elastic particles

In this section, the force-displacement relations of two contacted asperities are introduced. The Hertzian theory and the classical Mindlin law are applied for normal and tangential directions, respectively [23]. As shown in Fig. **2**, the contact between two spherical asperities can be simplified to a rigid plane's contact. The elastic spherical body has combined equivalent parameters of two contacting asperities. The tangential stiffness formulation, which is a function of the circular stick area's radius, is introduced in this section.

The normal force between two asperities with a penetration depth of w is defined using the Hertz relation as [18],

$$f_\upsilon = K\, w^{3/2},\ K = \frac{4}{3}\bar{E}\sqrt{\bar{R}}. \tag{1}$$

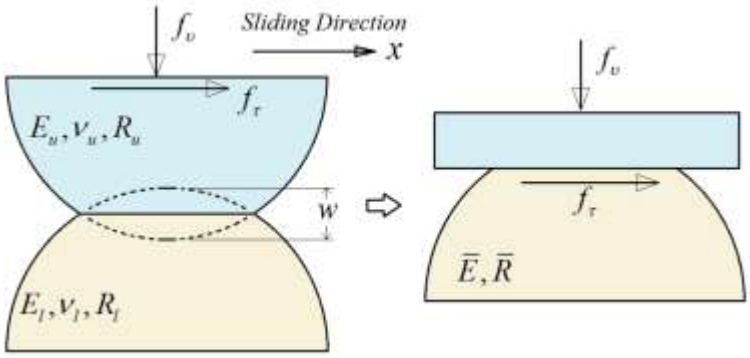

Fig. 2: Two contacting spherical particles and their equivalent contact model (reduced model).

where:

$$\bar{E} = \left((1-\nu_l^{\,2})E_l^{-1} + (1-\nu_u^{\,2})E_u^{-1}\right)^{-1},\ \bar{R} = (R_l^{-1} + R_u^{-1})^{-1}. \tag{2}$$

The symbols R_u, R_l denote the radius of upper and lower asperity summits. The Young moduli and the Poisson's ratio of the asperities are designated by E_u, E_l and ν_u, ν_l, respectively. Subscripts u and l denote the upper and lower surfaces. The radius of the contact area a equals,

$$a = (\bar{R}\, w)^{1/2}. \tag{3}$$

The distribution of normal pressure in the circular contact area is [23],

$$p(r) = p_0\left(1-\frac{r^2}{a^2}\right)^{1/2},\quad p_0 = \frac{3f_\upsilon}{2\pi a^2}. \tag{4}$$

The states of motion of the two contacted asperities may be pre-slip or macro-slip. In the pre-slip state, the middle part of the circular contact area is in stiction, while in the macro-slip state, the

stick area of asperities disappears [23]. Fig. **3** shows the distribution of normal pressure and tangential traction on the stick and the contact area.

The pre-slip motion of preloaded two contacted spherical bodies was worked out first by Cattaneo [25] and independently by Mindlin [26]. The classical Mindlin formulation of tangential friction force in the virgin loading phase at pre-slip is [23],

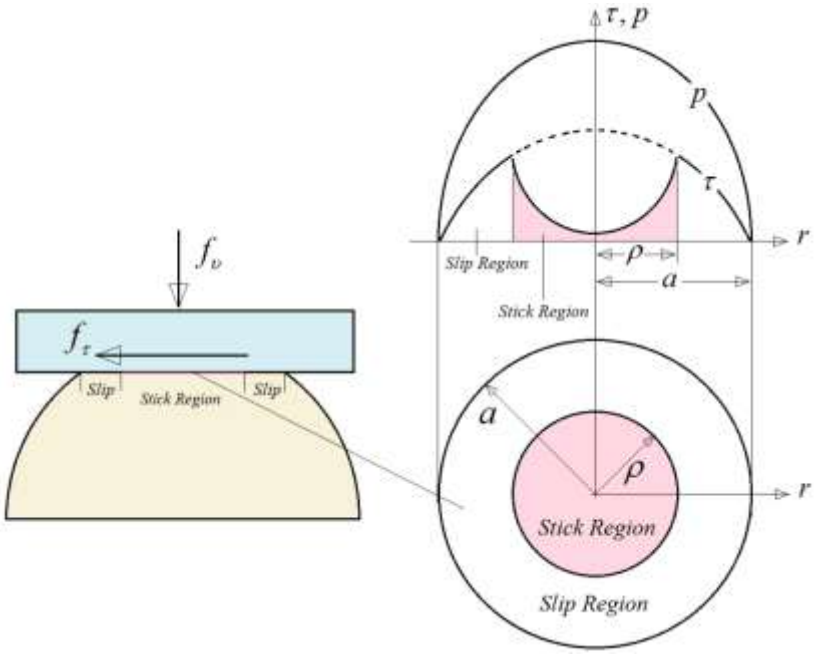

Fig. 3: Normal-pressure and tangential stress distribution of contact area and stick region in the contact of an elastic spherical asperity and a rigid plane.

$$f_\tau(x) = \mu f_\upsilon \left(1 - \left(1 - \frac{16\, a \bar{G}}{3 \mu f_\upsilon} x\right)^{3/2}\right), \quad \text{pre-slip state},$$
$$f_{slip} = \mu f_\upsilon, \quad \text{macro-slip state}. \tag{5}$$

In Equation (5), the parameter x denotes the relative tangential motion or elastic deformation and $\bar{G}$ is combined shear moduli, i.e.:

$$\bar{G} = \left((2-\nu_l)G_l^{-1} + (1-\nu_u)G_u^{-1}\right)^{-1}. \tag{6}$$

Shear moduli of the two contacting asperities are designated by G_u, G_l and μ denote the friction coefficient. Various friction coefficient types in asperity scales, such as constant friction coefficient and asperity penetration depth-dependent friction coefficient, are proposed in the literature [19]. Additionally, considering the lateral contact effect of the friction coefficient, a corrected constant friction coefficient is given as [22]:

$$\mu = \mathrm{S}/\mathrm{H} + 0.1, \tag{7}$$

where parameters S and H , are respectively, shear strength and hardness of softer material, and the value of 0.1 is an equivalent mean value of asperities' contact angles [22]. The constant friction coefficient of Equation (7) is applied in Equation (5). In the following, it is assumed that two asperities are of similar material properties and identical summit radius, i.e.:

$$\begin{aligned} R_l = R_u = R, \quad \nu_l = \nu_u = \nu. \\ E_l = E_u = E, \quad G_l = G_u = G. \end{aligned} \tag{8}$$

when two asperities are of similar material properties, one may write:

$$\bar{E} = \frac{E}{2(1-\nu^2)}, \quad \bar{G} = \frac{G}{2(2-\nu)}, \quad E = 2G(1+\nu). \tag{9}$$

Using Equation (5), the maximum tangential elastic deformation or maximum pre-slip displacement limit of two contacting asperities is determined by equating the stick and slip forces ($f_\tau(x_{slip}) = f_{slip}$), leading to:

$$x_{slip} = \frac{3\mu f_\upsilon}{16\,\bar{G}\,a}. \tag{10}$$

The maximum pre-slip displacement limit in Equation (10) is:

$$x_{slip} = \lambda w. \tag{11}$$

where:

$$\lambda = \mu\left(\frac{2-\nu}{2-2\nu}\right). \tag{12}$$

By substitution of Equation (11) into Equation (5), the tangential force-displacement relation of two contacting spherical particles is obtained,

$$f_\tau(x) = \mu f_\upsilon\left(1-\left(1-\frac{x}{\lambda w}\right)^{3/2}\right). \tag{13}$$

The tangential displacement relation in the pre-slip state of two contacted spherical particles as a function of the radius of the stick region area is [23],

$$x = \alpha\,(a^2-\rho^2), \quad \alpha = \frac{3\mu f_\upsilon}{16\bar{G}\,a^3} = \frac{\lambda w}{a^2}. \tag{14}$$

The stick area's radius approaches zero while the two contacting spherical asperities are at the macro-slip state. By substitution Equation (14) into Equation (13), the tangential friction force of two contacting asperities can be rewritten as a function of stick region radius [23],

$$f_\tau(\rho) = \mu f_\upsilon\left(1-\frac{\rho^3}{a^3}\right). \tag{15}$$

The tangential stiffness of two contacted asperities is defined as,

$$\mathrm{k}_{\tau}(x)=\frac{\partial f_{\tau}(x)}{\partial x}, \tag{16}$$

which leads to:

$$\mathrm{k}_{\tau}(x)=\frac{3\mu}{2\lambda}K\,w^{1/2}\left(1-\frac{x}{\lambda w}\right)^{1/2}. \tag{17}$$

Alternatively, the tangential stiffness of two contacting asperities as a function of stick region radius is as follows:

$$\mathrm{k}_{\tau}(\rho)=\frac{\partial f_{\tau}(\rho)}{\partial \rho}\left(\frac{\partial x}{\partial \rho}\right)^{-1}. \tag{18}$$

By substitution Equations (15) and (14) into Equation (18), a simple expression for the tangential contact stiffness is obtained [27],

$$\mathrm{k}_{\tau}(\rho)=8\bar{G}\,\rho. \tag{19}$$

Considering Equation (19), the initial tangential stiffness of two spherical asperities at the beginning of elastic deformation, i.e. $\rho=a$, is equal to:

$$\mathrm{k}_{\tau o}=8\bar{G}\,a. \tag{20}$$

The governing formulations of two contacting rough surfaces are introduced in the following section, assuming a constant friction coefficient.

2.2. Rough interface contact theory

This section introduces the rough interface contact model based on friction force displacement of two contacting asperities of Equation (13). In this correlation, the normal preloaded elastic asperities and constant friction coefficient model are integrated into the Cattaneo–Mindlin partial slip solution [19], known as the multi-asperity contact theory. In contacting two nominally flat rough surfaces, the contact occurs between asperities, and a distance between the reference planes is defined by the mean value of both surfaces' asperity heights. The assumption of parallelism of reference planes allows the rough interface to be equivalently represented as contact between a smooth, rigid, flat surface and a rough surface with combined roughness called a single rough surface model, as shown in Fig. **4** [18, 19].

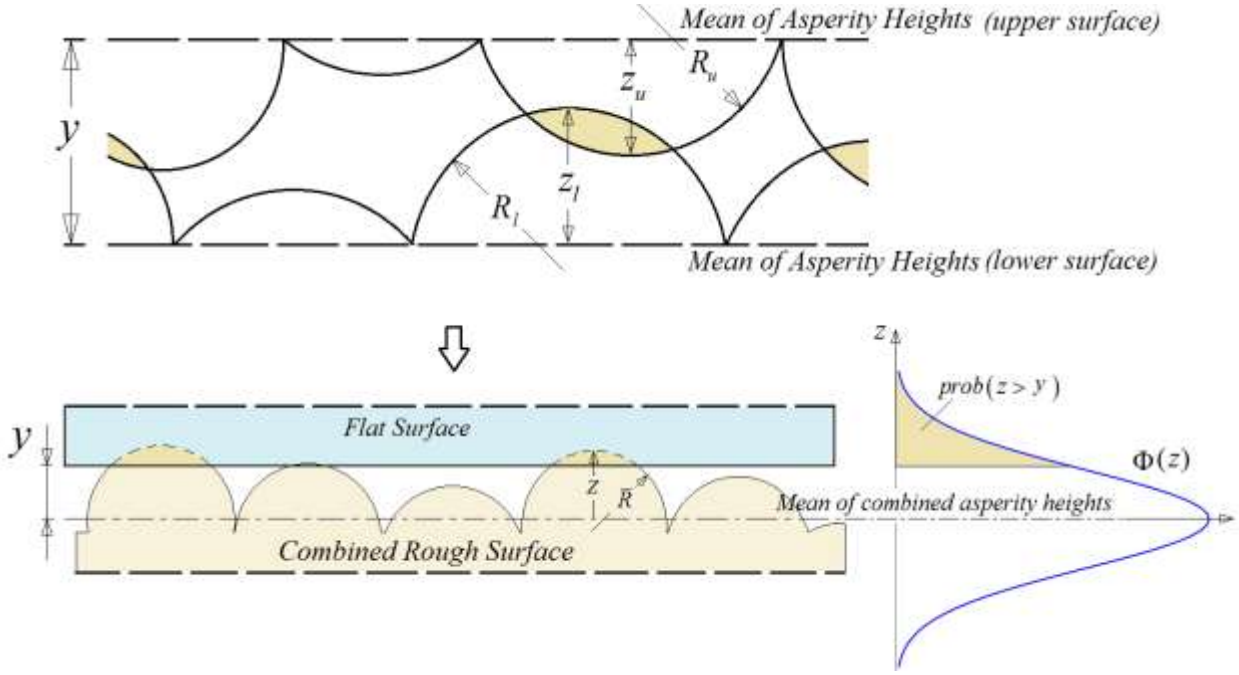

Fig. 4: Distribution of asperity heights of equivalent single rough surface contact model.

The SRS model's governing equation is introduced by the pre-determined distribution function of asperity heights and considering Hertzian and Mindlin's tangential force-displacement law. Asperity heights' distribution function is determined using roughness parameters such as kurtosis and skewness [28]. Various asperity heights' distribution functions are introduced in the literature; a Gaussian probability distribution function of combined roughness is defined as [17],

$$\Phi(z) = \frac{1}{\sqrt{2\pi}\sigma} Exp[-\frac{1}{2}(\frac{z}{\sigma})^2], \quad \left(z = z_u + z_l, \quad \sigma^2 = {\sigma_u}^2 + {\sigma_l}^2\right). \tag{21}$$

The parameters z and σ are the sum of asperity heights and combined standard deviations of asperity heights of two contacting rough surfaces, respectively. Alternatively, the exponential probability distribution function of the interface is defined as [29]:

$$\Phi(z) = \frac{\boldsymbol{\alpha}}{\sigma} Exp[-\boldsymbol{\beta}\frac{z}{\sigma}]. \tag{22}$$

In Equation (22), $\boldsymbol{\alpha}$ and $\boldsymbol{\beta}$ constant parameters are determined by the measured roughness profile. The asperity height distribution function is also defined following Demkin's power-law exponent as a function of the relative approach of contacting surfaces [30]. The combined rough surface parameters are calculated as functions of two contacting surfaces' roughness profiles [31]. The distance between two flat surfaces is denoted by y, and the penetration depth of each contacted asperities is as follows:

$$w = z - y. \tag{23}$$

The critical interference, w_c which defines the inception of elastic-plastic contact, is given by [32]:

$$w_c = \left(\frac{\pi \Omega \mathrm{H}}{2\bar{E}} \right)^2 \bar{R}\,, \quad \Omega = 0.454 + 0.41\nu. \tag{24}$$

When the normal interference $w < w_c$, the contact is deemed purely elastically deformed. The normal contact force is assumed to be low, where the deformation of mostly asperities is lower than w_c. The total number of asperities in the contact interface is $N_a = \eta A$, where η is the density of asperities distributed over the nominal contact area A. The number of contacting asperities is then determined as follows:

$$n_a = \eta \mathrm{A} \int_y^{\bar{z}_{\max}} \Phi(z)\, dz. \tag{25}$$

The parameter $\bar{z}_{\max}$ defines the upper bound of asperity heights. When using the Gaussian distribution function, it is assumed $\bar{z}_{\max} = 3\sigma$ to include almost all the contacted asperities. The normal force between two contacting surfaces F_υ is then obtained as [18]:

$$F_\upsilon(y) = \eta \mathrm{A} \int_y^{\bar{z}_{\max}} f_\upsilon\ \Phi(z)\ dz. \tag{26}$$

By substituting Equation (1) into Equation (26), the normal contact force is obtained as:

$$F_\upsilon(y) = K\eta \mathrm{A} \int_y^{\bar{z}_{\max}} (z-y)^{3/2}\ \Phi(z)\ dz. \tag{27}$$

On the other hand, the tangential friction force of two contacting rough surfaces in the virgin loading phase is [19],

$$Q_v(x,y) = \eta \mathrm{A} \int_y^{\bar{z}_l(x)} f_{slip}\, \Phi(z)\, dz + \eta \mathrm{A} \int_{\bar{z}_l(x)}^{\bar{z}_{\max}} f_\tau(x)\ \Phi(z)\, dz. \tag{28}$$

The variable $\bar{z}_l$ denotes the boundary of asperity heights for the slip and stick state of the elastic region and is determined by equating the slip and stick forces ($f_\tau\big|_{z=z_l} = f_{slip}$), i.e.,

$$\bar{z}_l(x) = y + \frac{x}{\lambda}. \tag{29}$$

Also, the tangential stiffness of the rough interface is obtained using Equations (28) and (16):

$$K_\tau^v(x,y) = \frac{\partial Q_v(x,y)}{\partial x} = \eta \mathrm{A} \int_{\bar{z}_l(x)}^{\bar{z}_{\max}} \mathrm{k}_{\tau,x}(x)\, \Phi(z)\, dz. \tag{30}$$

Substitution Equation (17) into Equation (30) determines the tangential stiffness of contacting surfaces at the beginning of the initial loading ($x = 0$).

$$K_T = K_\tau^v(x,y)\big|_{x=0} = \frac{3\mu}{2\lambda} K\eta \mathrm{A} \int_y^{\bar{z}_{\max}} (z-y)^{1/2}\ \Phi(z)\, dz. \tag{31}$$

Equation (31) defines the initial interface stiffness in the elastic contact region. Using the virgin loading phase of tangential force as a function of displacement denoted by $Q_v(x)$, the tangential friction force in the unloading and reloading phase is determined using the Masing rule [33],

$$\begin{aligned} Q(x)_{Reloding} &= -Q_o + 2Q_v\left(\frac{x+x_o}{2}\right). \\ Q(x)_{Unloading} &= Q_o - 2Q_v\left(\frac{x_o-x}{2}\right). \end{aligned} \tag{32}$$

The parameters Q_o and x_o are the amplitude of exciting force and the amplitude of tangential motion, respectively.

3. Determination of Maxwell slip model parameters

This section introduces the contacting rough interface equivalent to the Maxwell slip model, i.e., a parallel series of Jenkins elements. In other words, the SRS asperity scale model is converted to a Maxwell slip model. The Maxwell slip model for representing hysteresis behavior consists of a parallel connection of L massless elastoplastic elements known as Jenkins elements subject to a unified input velocity [34], as shown in Fig. **5**.

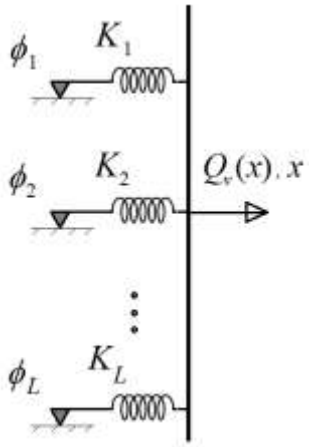

Fig. 5: Maxwell slip model.

A Jenkins element is characterized by its particular stiffness K_i and slippage friction force ϕ_i. Each element is assumed to be massless. During loading or relative motion, the element remains in the stick state until the spring deflection force exceeds the slippage force upon which the element begins to slide. In the slip state, the deflection force of the Jenkins element remains constant until the motion changes direction. The restoring force of a single Jenkins element in the virgin loading phase is:

$$q_i(x) = \begin{cases} K_i\, x & |q_i| < \phi_i, \\ \phi_i & \text{else}. \end{cases} \tag{33}$$

The superposition of elements restoring forces produces the total friction force:

$$Q_v(x) = \sum_{i=1}^{L} q_i(x). \tag{34}$$

The total tangential friction force in the unloading and reloading phase is determined using the virgin loading phase by applying the Masing rule of Equation (32). The smoothness of the friction force transition after each motion reversal depends on the number of elements employed in the Maxwell slip model. The Maxwell slip model becomes more accurate as more Jenkins elements are used. The parameters of the Maxwell slip model (K_i and ϕ_i) can be identified from experimental test data. In the following, an analytical method to determine the Maxwell slip model parameters is presented by matching the restoring forces of the contact determined by rough interface contact theory. A discrete model of the contact interface is formed by dividing the contact interface into *N* regions of similar height asperities to achieve this goal. The mean value of the contact area associated with each N height region is obtained. Based on the state of motion, the areas of each height region of contacting asperities are divided into *M* annulus elements, where each annulus element denotes a step of sliding motion. The slippage friction forces of annulus elements are obtained using a constant friction coefficient and a preload of each element based on the Hertzian distribution of normal pressure of Equation (4).

Moreover, each annulus element's stiffness at the asperity scale is obtained based on the Mindlin solution of Equation (19). Finally, the extracted relations on the asperity scale are developed using statistical summation for height regions and the whole rough interface. The slippage friction force and stiffness of each Jenkins element in the Maxwell slip model are determined using material properties and roughness parameters of contacting surfaces. The proposed procedure leads to the analytical development of a frictionally rough interface model. The following verifies the accuracy of the developed Maxwell model's predictions using the proposed process of contact modeling against the analytical multi-asperity contact model introduced in Section 2. Also, it investigates the effect of the selected number of similar height-region *N* and *M* annulus elements on the quality and accuracy of predicted hysteresis friction curves.

3.1. Equivalent Maxwell slip model on asperity scale

In the asperity scale, the contact is represented using a parallel series of Jenkins elements by dividing the contact area into annuluses, as a sample denoted by width $\Delta\rho_m$ in Fig. 6, where index *m* is the annulus counter.

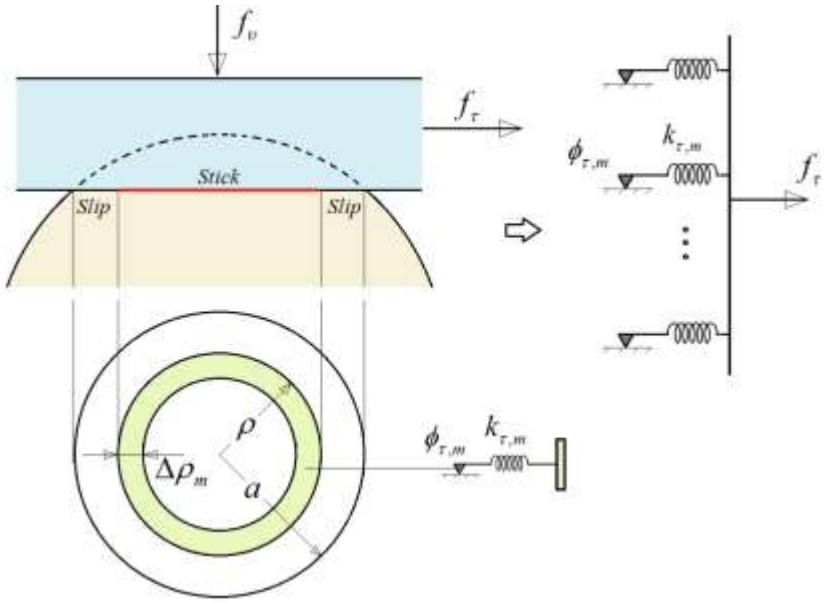

Fig. 6: Equivalent Maxwell slip model of a reduced model of two contacting asperities.

The normal pressure distribution, tangential force-displacement, contact deformation, and radius of the stick region of the mean contact area established in Section 2 determine each Jenkins element's stiffness and slippage friction force. As shown in Fig. **3** and Fig. **6**, during the tangential relative motion of two contacted asperities, the state motion of the circular contact area is changed from stiction to macro-slip state. In the initial loading, the stick region's radius is equal to the radius of the contact area, i.e., the entire area is in the stick state ($\rho = a$). Also, during relative motion, the x value varies from zero to x_{slip}, i.e., ($x : 0 \to x_{slip}$), and the radius of the stick region approaches zero, i.e. ($\rho \to 0$). Equation (19) established that contacting asperities' tangential stiffness is proportional to the stick region's radius. Therefore, the tangential stiffness softening is proportional to the stick region radius reduction during the tangential motion in constant normal load conditions. According to Equations (19) and (20), the tangential stiffness softens from $\mathrm{k}_{\tau o}$ to zero. In general, the variation of tangential stiffness between ρ , and $\rho + \Delta\rho$, is determined as:

$$\Delta \mathrm{k}_\tau \left(\rho \to \rho + \Delta\rho \right) = 8\bar{G}\, \Delta\rho. \tag{35}$$

The region of the contacting area is divided into arbitrary M annulus elements located between the radius.

$$\vec{\rho} = \left\{ r \right\}_M = \left\{ r_0 \quad r_1 \quad \ldots \quad r_m \quad \ldots \quad r_{M-1} \quad r_M \right\}^T, \quad \left(r_0 = 0,\, r_M = a \right). \tag{36}$$

Then, the tangential stiffness of the annulus elements, shown in Fig. **6**, are as follows:

$$\mathrm{k}_{\tau,m} = \Delta \mathrm{k}_\tau \big|_{\rho:\, r_{m-1} \to r_m} = 8\bar{G}\, \Delta r_m, \quad \Delta r_m = r_m - r_{m-1}, \quad m = 1, 2, \ldots, M. \tag{37}$$

Also, the equivalent normal force of each annulus element, considering pressure distribution defined in Equation (4), is:

$$f_{\upsilon,m} = 2\pi \int_{r_{m-1}}^{r_m} p(r)\, r\, dr. \tag{38}$$

Considering Equation (38), the slippage friction force or the critical strength of each Jenkins element is:

$$\phi_{\tau,m} = \mu\, f_{\upsilon,m}, \quad m = 1,2,...,M. \tag{39}$$

By employing Equations (39) and (37), the equivalent parallel series of Jenkins elements of two contacted asperities is developed. In a numerical example, the resultant hysteresis friction force obtained by the proposed equivalent Maxwell slip model of two contacting asperities is determined for stick and macro-slip states. The normalized hysteresis friction forces are compared with Mindlin's solution of Equation (13) in virgin loading and unloading/reloading phases generated by the Masing rule of Equations (32). The results are shown in Fig. **7** to Fig**. 9** for different combinations of annulus elements. The resultant hysteresis friction curves in stick and macro-slip state, produced using M=3, M=7, and M=15 Jenkins elements, are shown respectively in Fig. **7**, Fig**. 8**, and Fig**. 9**, where the x and y-axes are normalized to slippage displacement limit and slippage friction force, respectively.

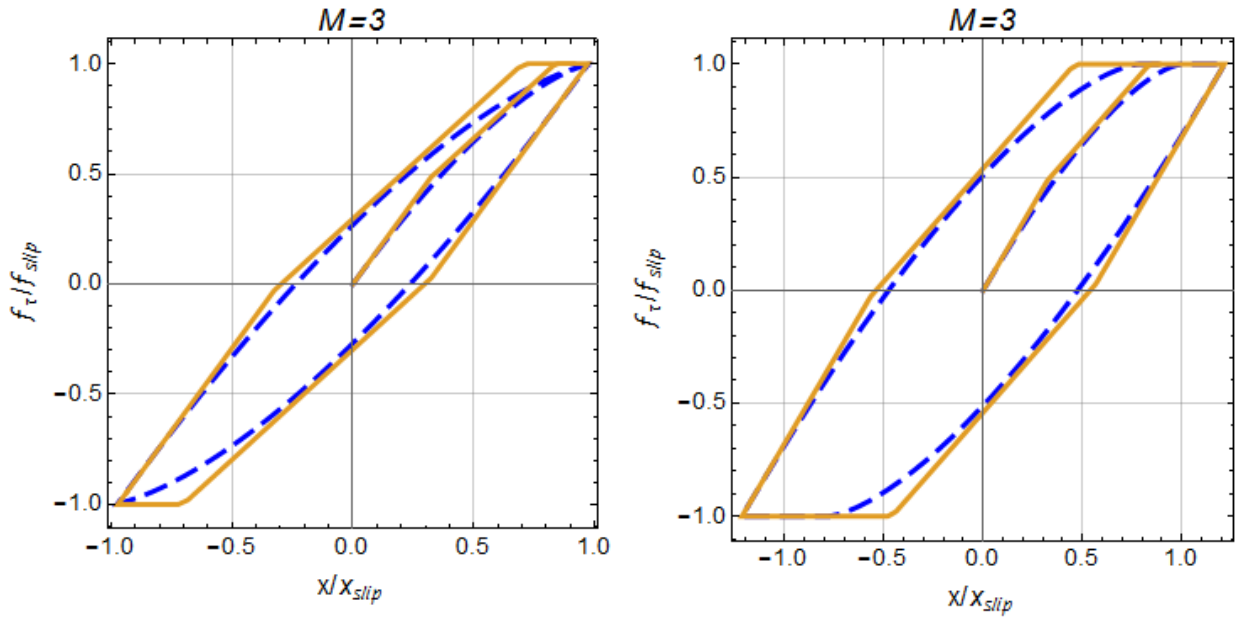

(a) (b)

Fig. 7: Normalized hysteresis curves determined by equivalent Maxwell slip model of two contacted asperities (solid line) and analytical model (dashed line): (a) pre-slip state, (b) macro-slip state.

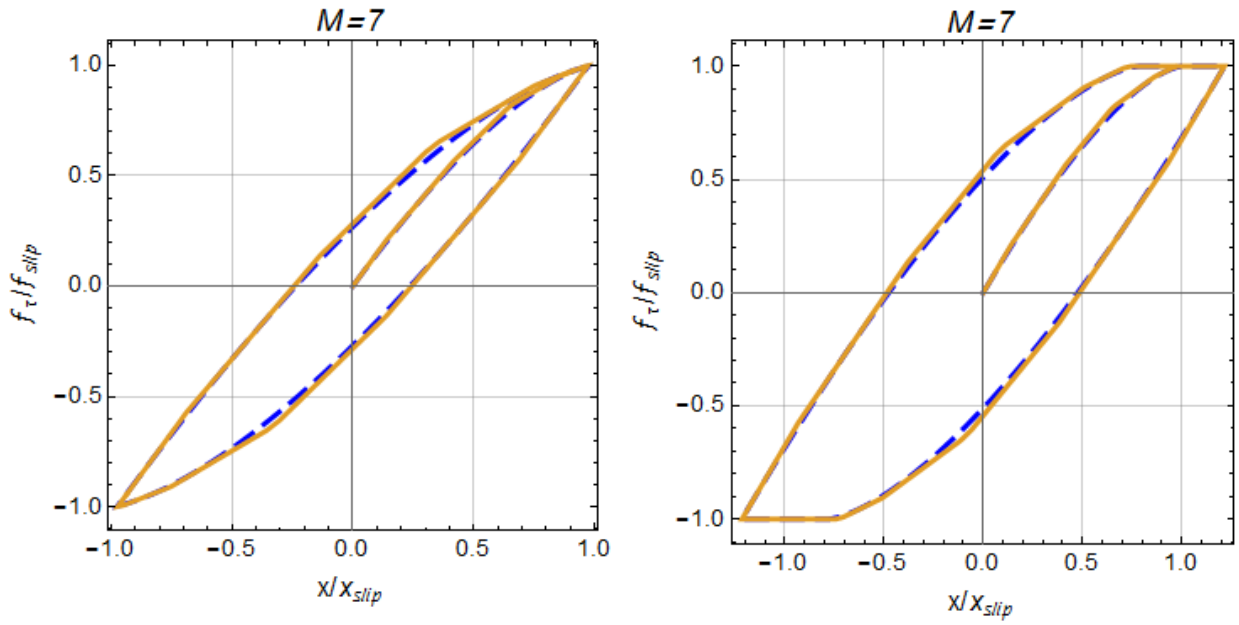

(a) (b)

Fig. 8: Normalized hysteresis curves determined by equivalent Maxwell slip model of two contacted asperities (solid line) and analytical model (dashed line): (a) pre-slip state, (b) macro-slip state.

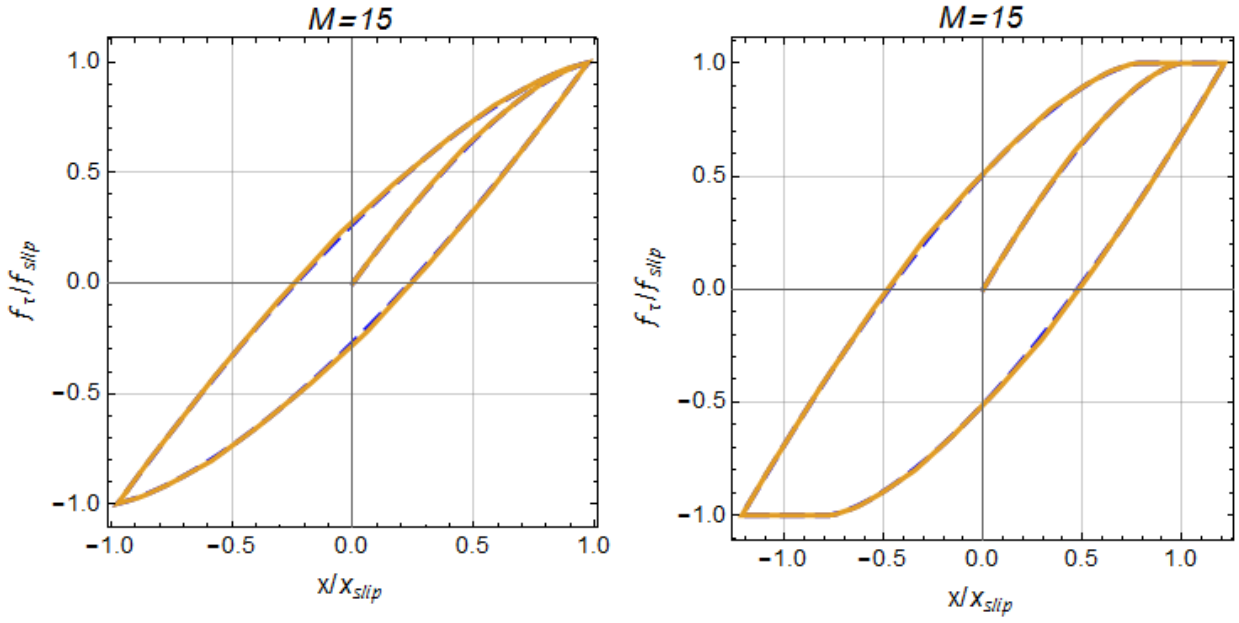

(a) (b)

Fig. 9: Normalized hysteresis curves determined by equivalent Maxwell slip model of two contacted asperities (solid line) and analytical model (dashed line): (a) stick state, (b) macro-slip state.

The results show that the determined equivalent Maxwell slip model with enough finite number of Jenkins elements accurately simulates two contacting asperities' frictional hysteresis behavior.

Therefore, a reliable, discrete model of the rough interface based on the defined Maxwell slip model on the asperity scale is established.

3.2.Equivalent Maxwell slip model of the rough interface

This section develops an equivalent parallel series of Jenkins elements of two contacting rough surfaces, as represented in Fig. **10**. The equivalent Maxwell slip model parameters of the whole rough interface, especially the stiffness and slippage friction force of Jenkins elements, are obtained using the interface material properties and roughness parameters.

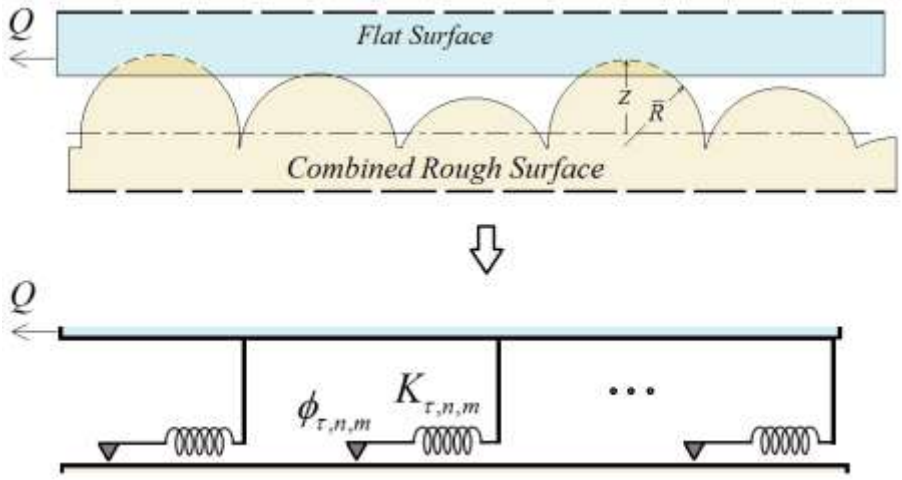

Fig. 10: SRS model and its equivalent Maxwell slip model.

The roughness parameters include asperity height standard deviations σ, the mean value of the asperity summit radius $\overline{R}$, and the areal asperity density η. As shown in Fig. **11**, the distribution of contacted asperity heights is divided into desired height regions,

$$\vec{\mathbf{Z}} = \{z_n\}_N = \{z_0 \quad z_1 \quad \dots \quad z_n \quad \dots \quad z_{N-1} \quad z_N\}, \quad (z_0 = y,\ z_N = \overline{z}_{\max}). \tag{40}$$

Using the mean value of the contact area radius of two contacted asperities of each region and employing the proposed strategy in Section 3.1, the annulus elements and the parameters of Jenkins elements of each height region are determined.

The number of asperities involves between heights z_{n-1}, and z_n, are,

$$N_{a,n} = N_a \int_{z_{n-1}}^{z_n} \Phi(z)\, dz, \quad n = 1,2,...,N. \tag{41}$$

Also, the normal contact force of asperities in the range of z_{n-1} and z_n is,

$$F_{\upsilon,n}(y) = K\eta\, \mathrm{A} \int_{z_{n-1}}^{z_n} (z-y)^{3/2}\ \Phi(z)\ dz, \quad n = 1,2,...,N, \tag{42}$$

and the interface total preload is the sum of these asperities' normal contact forces,

$$F_{\upsilon}(y)=\sum_{n=1}^{N}F_{\upsilon,n}(y). \tag{43}$$

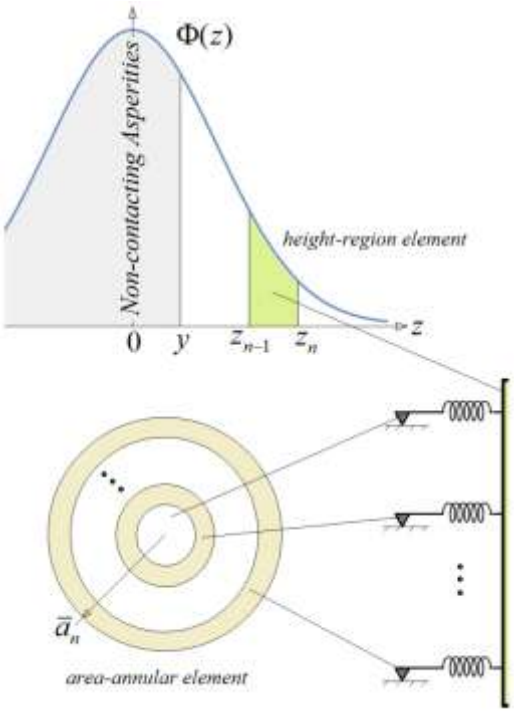

Fig. 11: Asperity height distribution function and annulus and height-region elements.

Considering Equations (3) and (23), the radius of the contact area of two contacting asperities is,

$$a(z)=\sqrt{\bar{R}}(z-y)^{1/2}. \tag{44}$$

The mean value of the radius of the contact area in the region located between z_{n-1}, and z_n, is obtained as follows:

$$\bar{a}_n=\frac{\int_{z_{n-1}}^{z_n}a(z)\ \Phi(z)\,dz}{\int_{z_{n-1}}^{z_n}\Phi(z)\,dz},\quad n=1,2,...,N. \tag{45}$$

By substitution Equation (41) into Equation (45), the radius of the contact area within each region is rewritten as:

$$\bar{a}_n=\frac{N_a}{N_{a,n}}\sqrt{\bar{R}}\int_{z_{n-1}}^{z_n}(z-y)^{1/2}\ \Phi(z)\,dz,\qquad n=1,2,...,N, \tag{46}$$

For N=1, the mean value of the contact area radius of all contacting asperities is obtained as:

$$\bar{a}=\frac{N_a}{n_a}\sqrt{\bar{R}}\int_{y}^{\bar{z}_{\max}}(z-y)^{1/2}\ \Phi(z)\,dz. \tag{47}$$

Therefore, using Equations (4), (42), and (46), the normal pressure distribution on the mean contact radius $\bar{a}_n$ is,

$$\mathrm{P}_n(r) = P_0\left(1-\frac{r^2}{\bar{a}_n{}^2}\right)^{1/2}, \quad P_0 = \frac{3F_{\upsilon,n}}{2\pi\,\bar{a}_n{}^2}, \quad n=1,2,...,N. \tag{48}$$

The annulus elements associated with the mean contact area radius are developed in the next step. Similar to Equation (38) and considering Equation (48), the equivalent normal force of each annulus element is assigned as:

$$F_{\upsilon,n,m} = 2\pi\int_{r_{m-1}}^{r_m} \mathrm{P}_n(r)\; r\,dr, \quad n=1,2,...,N,\;\; m=1,2,...,M. \tag{49}$$

The bounds of the integral are similar to Equation (36), defined by discretizing the contact interface to *M* elements,

$$\vec{\boldsymbol{\rho}} = \{r\}_M = \{r_0 \quad r_1 \quad ... \quad r_m \quad ... \quad r_{M-1} \quad r_M\}, \;\; (r_0 = 0,\; r_M = \bar{a}_n). \tag{50}$$

Finally, considering Equation (49), similar to Equation (39), the slippage friction force of each Jenkins element is obtained,

$$\phi_{\tau,n,m} = \mu\, F_{\upsilon,n,m}, \quad n=1,2,...,N,\;\; m=1,2,...,M. \tag{51}$$

The following obtain the stiffness formulation of each Jenkin element. Using Equation (19), the total tangential stiffness of asperities within the range of z_{n-1}, and z_n, is defined as,

$$K_{\tau,n}(\rho) = \eta \mathrm{A}\int_{z_{n-1}}^{z_n} \mathrm{k}_{\tau,x}(\rho)\,\Phi(z)\,dz, \quad n=1,2,...,N, \tag{52}$$

or simply as,

$$K_{\tau,n}(\rho) = 8N_{a,n}\bar{G}\,\rho, \quad n=1,2,...,N. \tag{53}$$

The initial tangential stiffness of contacting asperities within the range of z_{n-1} and z_n is obtained from Equation (20),

$$\begin{aligned} &K_{0,n} = 8\bar{G}\,a_n. \\ &a_n = \eta \mathrm{A}\int_{z_{n-1}}^{z_n} a(z)\;\Phi(z)\,dz, \quad n=1,2,...,N. \end{aligned} \tag{54}$$

The tangential stiffness of contacting asperities at each region and its initial value may be simplified using Equations (41), (45), and (54) as,

$$K_{0,n} = 8\bar{G}\,N_{a,n}\,\bar{a}_n, \tag{55}$$

$$K_{\tau,n}(\rho) = K_{0,n}\frac{\rho}{\bar{a}_n}, \quad n=1,2,...,N. \tag{56}$$

Similar to Equation (37), the tangential stiffness of each annulus element $\Delta r_{m,n}$ is calculated as,

$$K_{\tau,n,m} = K_{0,n}\frac{\Delta r_{m,n}}{\bar{a}_n},\ \ \Delta r_{m,n} = r_m - r_{m-1},\ n = 1,2,...,N,\ \ m = 1,2,...,M. \tag{57}$$

Therefore, applying Equations (51) and (57), the rough interface contact can be converted to a parallel series of Jenkins elements, with *M* annulus elements at *N* height regions. As shown in Fig. **12**, the total number of discrete elements is equal to $L = N \times M$.

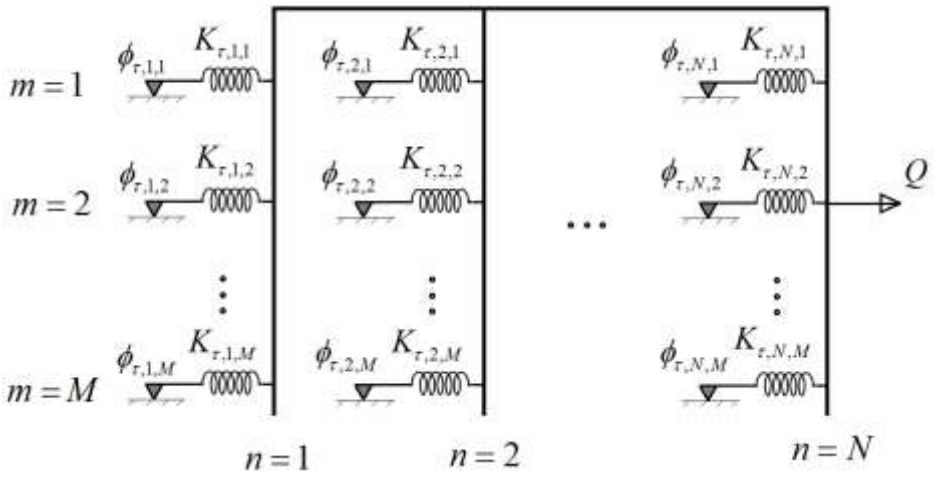

Fig. 12: A presentation of equivalent Maxwell slip model of rough interfaces.

The following numerical example demonstrates the resultant hysteresis friction curves determined using rough interfaces' equivalent Maxwell slip model. The results are obtained for stick and macro-slip states using the parameters of Table 1 and considering a preload of 100N.

Table 1: The rough interface contact parameters $(i = u, l)$.

Parameter:	σ_i	R_i	η_i	A
Value:	$1\mu m$	$200\mu m$	$250\,mm^{-2}$	$5\,cm^2$
Parameter:	E	ν	μ	
Value:	$200\,Mpa$	0.3	0.45	

The hysteresis curves are shown in Fig. **13** to Fig**. 15** for different numbers of Jenkins elements. Various *M* and *N* combinations are compared with the analytical multi-asperity contact model introduced in Section 2.2. Fig. **13** and Fig**. 14** indicate the discrete model results converge to those of the continuous model with a small number of *M* and an increasing number of *N*. Also, Fig. **15** shows that increasing *M* improves the model predictions.

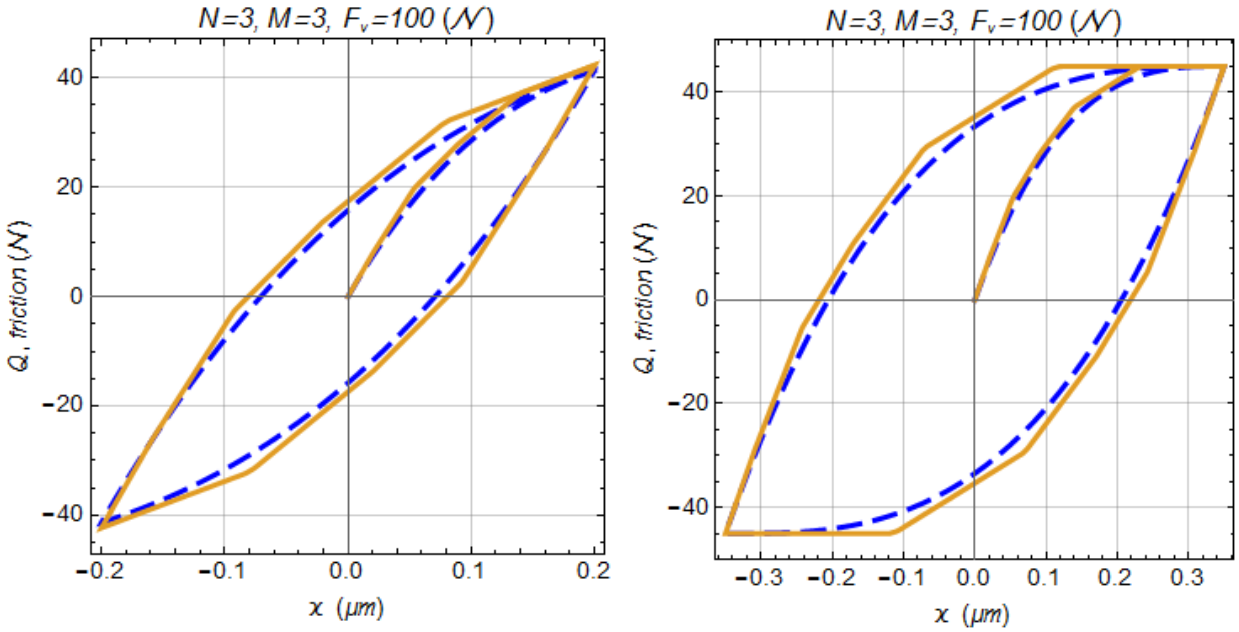

(a) (b)

Fig. 13: Comparison of resultant hysteresis curves of the equivalent Maxwell slip model (solid line) and analytical rough interface model (dashed line): (a) stick state, (b) macro-slip state.

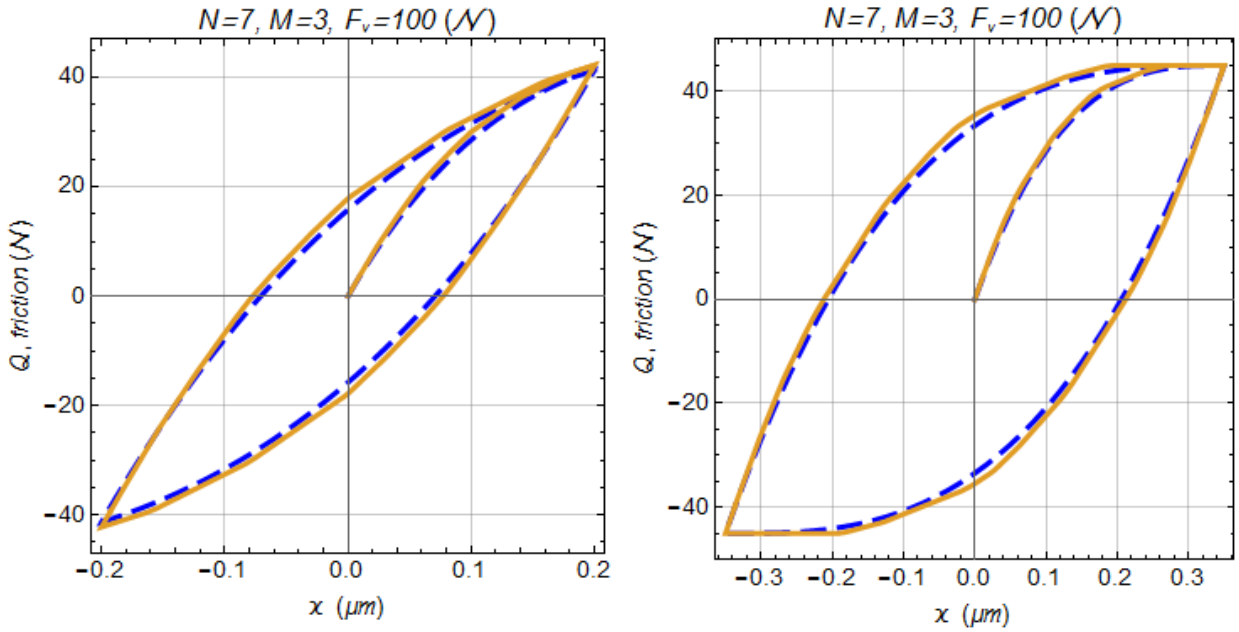

(a) (b)

Fig. 14: Comparison of resultant hysteresis curves of the equivalent Maxwell slip model (solid line) and analytical rough interface model (dashed line): (a) stick state, (b) macro-slip state.

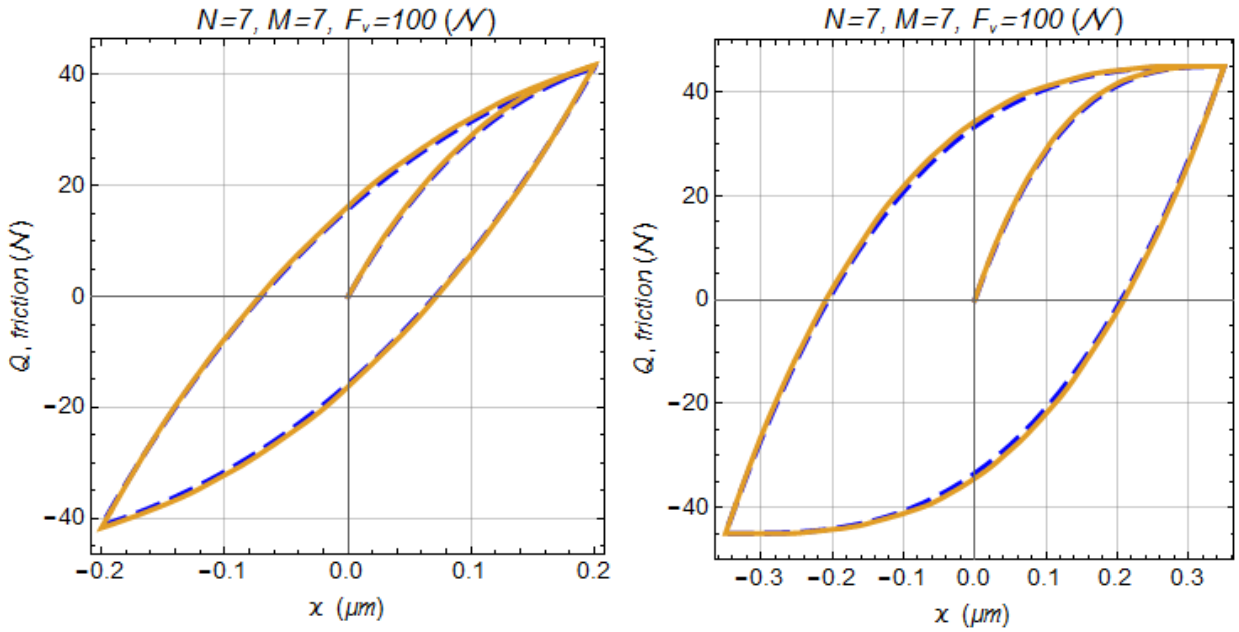

(a) (b)

Fig. 15: Comparison of resultant hysteresis curves of the equivalent Maxwell slip model (solid line) and analytical rough interface model (dashed line): (a) stick state, (b) macro-slip state.

Fig. **15** shows that, for a large number of *M* and *N*, the determined equivalent Maxwell slip model is in perfect agreement with the multi-asperity contact model. The equivalent Maxwell slip model of the considered rough interface is formed by L=21 Jenkins elements using two discrete models. The first model assumes N=7, M=3; the second adopts N=3, M=7. As shown in Fig. **16**(a), the resultant hysteresis friction forces are almost equal. One may infer that as the numbers *M* and *N* are greater than a specific value that includes all possible states of the contact surface, the discrete model produces acceptable models. The equivalent Maxwell slip model of the rough interface is also produced by L=30 Jenkins elements, using two combinations (N=1, M=30*)* and (N=3, M=10*)*. As shown in Fig. **16**(b), the reduction of the *N* value (i.e., N<3) removes the possibility of representing all the states of interface movements. This causes a significant error in the hysteresis friction curves.

Considering the results presented in Fig. **13** to Fig**. 16**, the number of Jenkins elements affects the smoothness and accuracy of hysteresis friction curves; in the first case, with 21 Jenkins elements, a good agreement with the reference data is observed (see Fig. **14**). When 49 Jenkins elements are considered, the hysteresis friction curves are more accurate, as shown in Fig. **15**. Therefore, for the contact surface described in Table 1, *N*'s value must be equal to or greater than 3 ($N \geq 3$), and the number of Jenkins elements must fall within the range $20 \leq L \leq 50$ for a reasonable hysteresis friction force (maximum 1% deviation in the hysteresis loop area),

So far, the equivalent parallel system of Jenkins elements of rough frictional interfaces is presented. The parameters of Jenkins elements, such as stiffness and critical slippage forces, are determined as functions of material properties and rough surface parameters, i.e.:

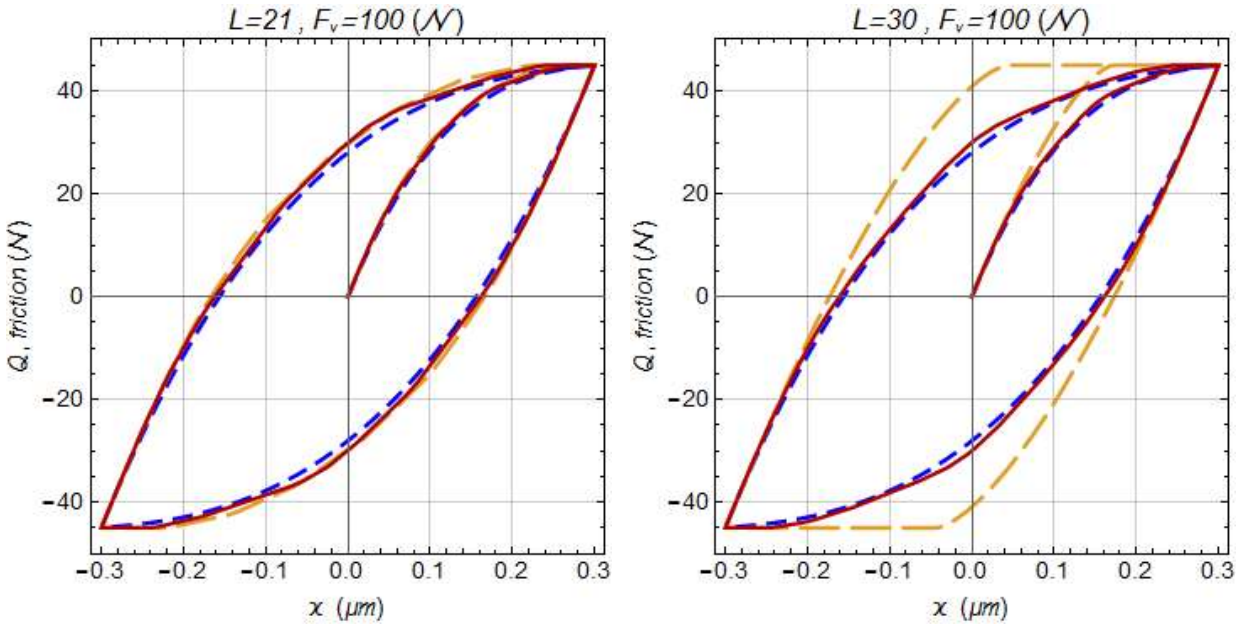

(a) (b)

Fig. 16: Comparison of resultant hysteresis curves of analytical rough interface model (short dashed line) and equivalent Maxwell slip model by:

(a) 21 Jenkins elements N=7, M=3 (solid line), N=3, M=7 (long dashed line), (b) 30 Jenkins elements N=3, M=10 (solid line), N=1, M=30 (long dashed line).

$$\phi_{\tau,n,m} = f_1(E,\nu,\sigma,\eta,R).$$
$$K_{\tau,n,m} = f_2(E,\nu,\sigma,\eta,R). \tag{58}$$

The resultant hysteresis curves show that the proposed Maxwell slip model perfectly agrees with the analytical multi-asperity theory. The summary of the determination process of the equivalent Maxwell slip model of an elastic frictional rough interface is given in Appendix A.

4. Continuous Iwan model of the rough interface

This section compares the proposed Maxwell slip model's performance in simulating the friction behavior of the rough interface against the continuous Iwan model. The continuous Iwan model comprises infinite Jenkins elements and is characterized by the slippage force (critical strength) distribution function. In the continuous Iwan model, the stiffness of all Jenkins elements is identical, and the total tangential friction force is calculated using the slippage distribution function $\tilde{\rho}(\phi)$ as [1]:

$$Q_v(x) = \int_0^{kx} \phi\tilde{\rho}(\phi)\,d\phi + kx\int_{kx}^{\infty}\tilde{\rho}(\phi)\,d\phi. \tag{59}$$

The variables ϕ and k denote the slippage force and stiffness value of the Jenkins elements, respectively. The continuous Iwan model can be extracted from the SRS model of multi-asperity contact theory [35]. Argatov and Butcher [30] determined the Iwan model as a function of the

relative approach of contacting surfaces. Using the contact shear force defined in Equation (28), the distribution function of slippage force in the continuous Iwan model can be expressed as [1]:

$$\tilde{\rho}(\phi) = -\frac{1}{k^2}\frac{\partial^2 Q_v}{\partial x^2}\bigg|_{\phi=kx}. \tag{60}$$

The parameter k can be removed from Equation (60) through the following changes of variable [5]:

$$\phi = k\,\varphi\ , \quad \rho(\varphi) = k^2\ \tilde{\rho}(\phi). \tag{61}$$

The maximum slippage force of Jenkins elements of the continuous Iwan model is,

$$\phi_{\max} = k\,x_L, \tag{62}$$

where x_L denotes the slippage displacement limit of the rough interface. Considering Equations (61) and (62), it can be written:

$$\varphi_{\max} = x_L. \tag{63}$$

By substitution of Equation (61) into Equation (60), the slippage distribution function of the continuous Iwan model is expressed as:

$$\rho(\varphi) = -\frac{\partial^2 Q_v(x)}{\partial^2 x}\bigg|_{\varphi=x}. \tag{64}$$

By substitution of Equation (26) into Equation (64), the second derivative of tangential contact force is obtained,

$$\frac{\partial^2 Q_v}{\partial x^2} = \eta \mathrm{A}\int_{\bar{z}_l(x)}^{\bar{z}_{\max}} \frac{\partial^2 f_\tau(x)}{\partial x^2}\ \Phi(z)\,dz. \tag{65}$$

The Iwan distribution function is obtained by substituting Equation (13) into Equation (65),

$$\rho(\varphi) = \frac{3\mu}{4\lambda^2} K\eta \mathrm{A}\int_{\bar{z}_l(\varphi)}^{\bar{z}_{\max}} (w-\frac{\varphi}{\lambda})^{-1/2}\,\Phi(z)\,dz, \quad \bar{z}_l(\varphi) = y+\frac{\varphi}{\lambda}. \tag{66}$$

It can be shown that the Iwan distribution function of Equation (66) is in agreement with Argatov and Butcher's proposal [30] (see Appendix B for more details). The Iwan distribution function $\rho(\varphi)$ can calculate the contact friction force as follows:

$$Q_v(x) = \int_0^x \varphi\,\rho(\varphi)\,d\varphi + x\int_x^\infty \rho(\varphi)\,d\varphi. \tag{67}$$

It is noted that $\rho(\varphi) = 0$ for $\varphi \geq \varphi_{\max}$. As a numerical study, the rough interface defined by Table 1 is considered, and its associated Iwan distribution function is determined. The contact hysteresis friction curves are plotted and compared with the resultant curve obtained by the multi-asperity contact model in Section 2. Fig. **17** shows the normalized distribution function of the slippage friction force of the infinite number of Jenkins elements; the figure axes are normalized to the maximum slippage force and boundary value of the slippage distribution function, respectively.

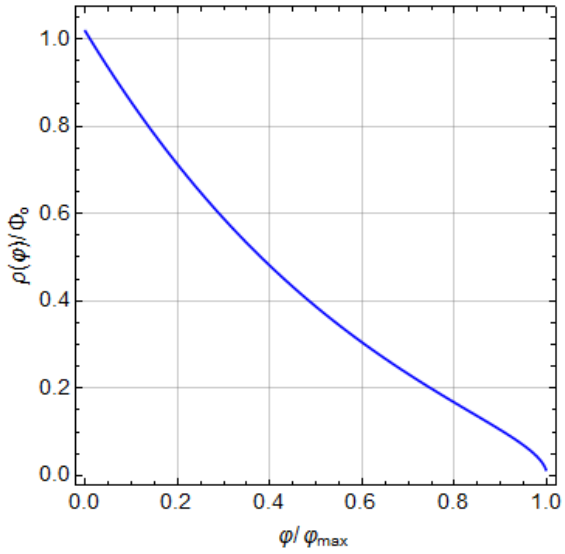

Fig. 17: Normalized Iwan distribution function of rough interfaces.

The boundary value of the slippage distribution function at $\varphi = 0$, denoted by Φ_0, is determined using Equation (66) as,

$$\rho(\varphi)\big|_{\varphi=0} = \Phi_0, \quad \Phi_0 = \frac{3\mu}{4\lambda^2} K\eta A \int_y^{\bar{z}_{max}} (z-y)^{-1/2} . \Phi(z)\, dz. \tag{68}$$

The obtained Iwan distribution function precisely simulates the frictional behavior of rough interfaces, as shown in Fig. **18**.

According to Fig. **15** and Fig**. 18**, it can be concluded that the resultant hysteresis friction curves by the Maxwell slip model with an appropriate number of Jenkins elements (L=49) and the continuous Iwan model are identical, i.e., their performance is the same, and these models can be used interchangeably.

5. Experimental case study

In this section, two test setups and experimental observations are employed to verify the proposed discrete Maxwell slip and the continuous Iwan models. In the first setup, the frictional contact of two aluminum blocks is under uniform preload, while the second setup is composed of a beam with frictional support [15, 36, 37]

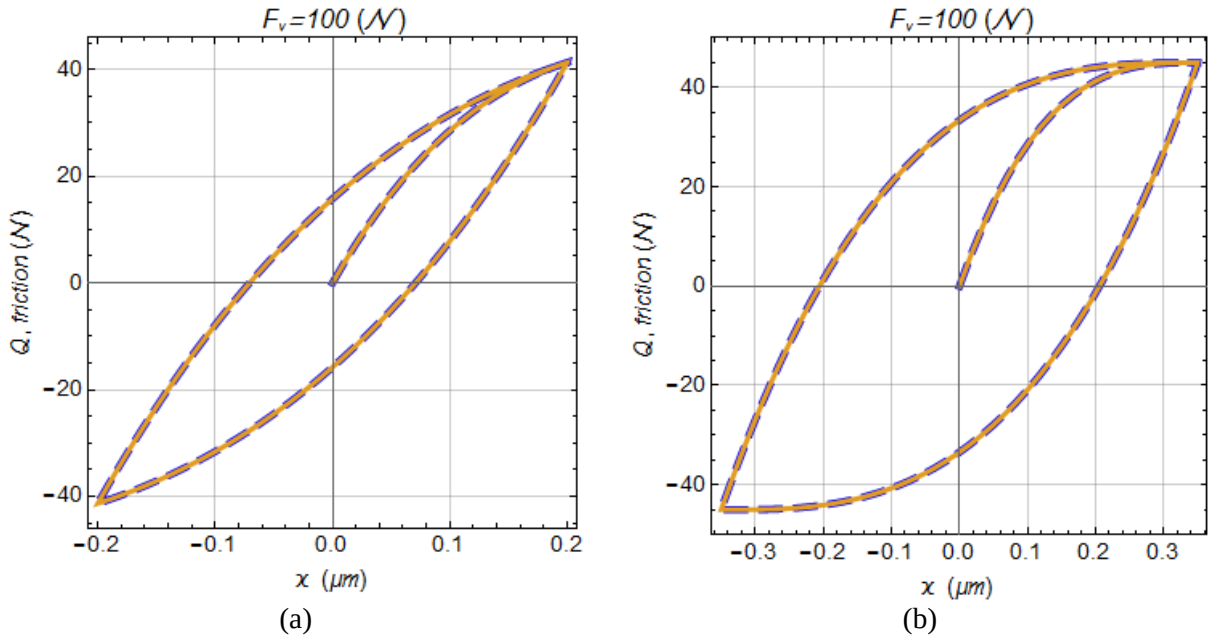

(a) (b)

Fig. 18: Hysteresis curves of the obtained Iwan distribution function (solid line) and rough interface model (dashed line): (a) stick state, (b) macro-slip state.

5.1. The frictional contact of two aluminum blocks

As shown in Fig. **19** and Fig. **20**, the test setup consists of two aluminum mass blocks with frictional contact. The upper block was attached to a linear spring and slipped on the lower aluminum mass block surface [38, 39]. The contacting surfaces are carefully machined to achieve a uniform roughness, as specified in Table 2.

Table 2: Surface roughness parameters of aluminum block and material properties.

Parameter:	σ_i	R_i	η_i	A
Value:	$0.85\mu m$	$170\mu m$	$210\times10^{-6}\ \mu m^{-2}$	$100\,cm^2$
Parameter:	E	v	S/H	
Value:	$70\,Mpa$	0.3	0.16	

The contact preload was equal to the weight of the upper block of mass 2 Kg. A suspended B&K mini shaker, Type 4810, excites the mass block. A B&K 8200 force transducer between the shaker and the metal block measures the in situ force in the excitation direction throughout the experiments. A DJB A/120/V accelerometer measures the movement of the upper block, and an NI DAQ USB-4431dynamic signal acquisition device is used to condition the measured data.

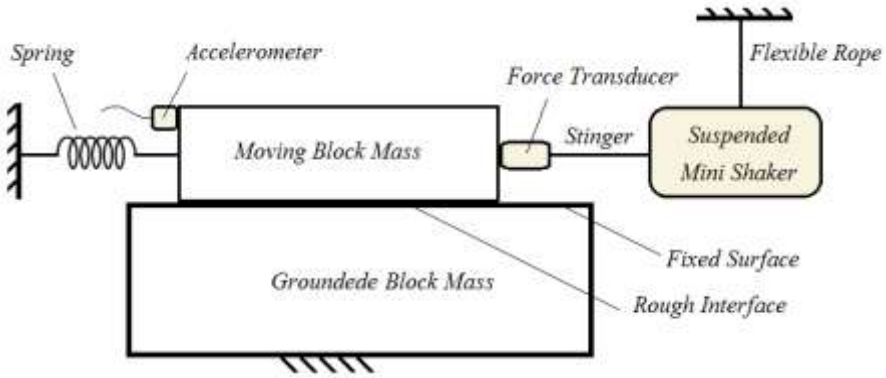

Fig. 19: Schematic of the test setup.

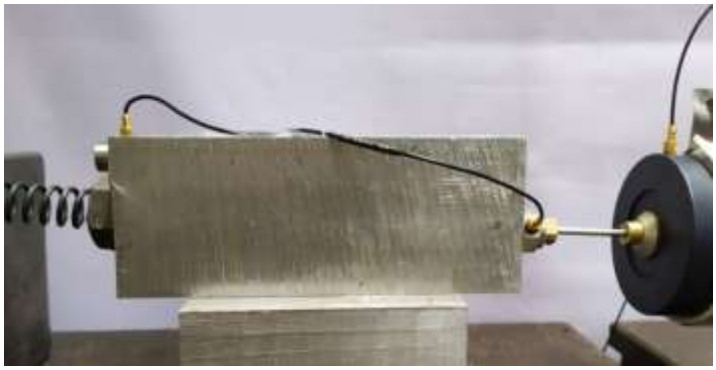

Fig. 20: Experimental test setup of the rough interface.

The measured response of the test setup to a simple harmonic excitation of 65 Hz is shown in Fig. **21**. The contact friction force $Q(x)$ was obtained by subtracting the spring force and inertia force of the mass block from the excitation force as:

$$Q(x) = F_{excite} - M\ddot{x} - K_S x. \tag{69}$$

In Equation (69), M refers to the upper block mass, and the spring stiffness K_s is known. The resultant hysteresis loops of the test setup excited with a simple harmonic force at the frequency of 65 Hz are shown in Fig. **22**. As mentioned in Section 2, the rough contacting surfaces are not completely elastic at first. Some roughness undergoes initial plastic deformation due to the vibrational load of interface and sliding, and after initial vibrational loading, the rough surface will be completely stable. Based on this, the initial measurement data and the obtained hysteresis loop are not smooth, but they become smooth during sliding due to vibration. Here, the test sample was subjected to an initial vibrational load. Then, when the measured acceleration of the samples at the excitation frequency of the shaker reaches a stable and smooth state (after about 5 minutes of vibrational excitation), the shaker excitation force and acceleration of the test sample are measured and recorded as validation criteria. Therefore, as observed in Fig. **21**, the shaker force and displacement in the time domain will be smooth. Subsequently, the hysteresis curve obtained from plotting force vs displacement of Fig. **22** will be smooth in the entire diagram, even the beginning and end points of the hysteresis graph.

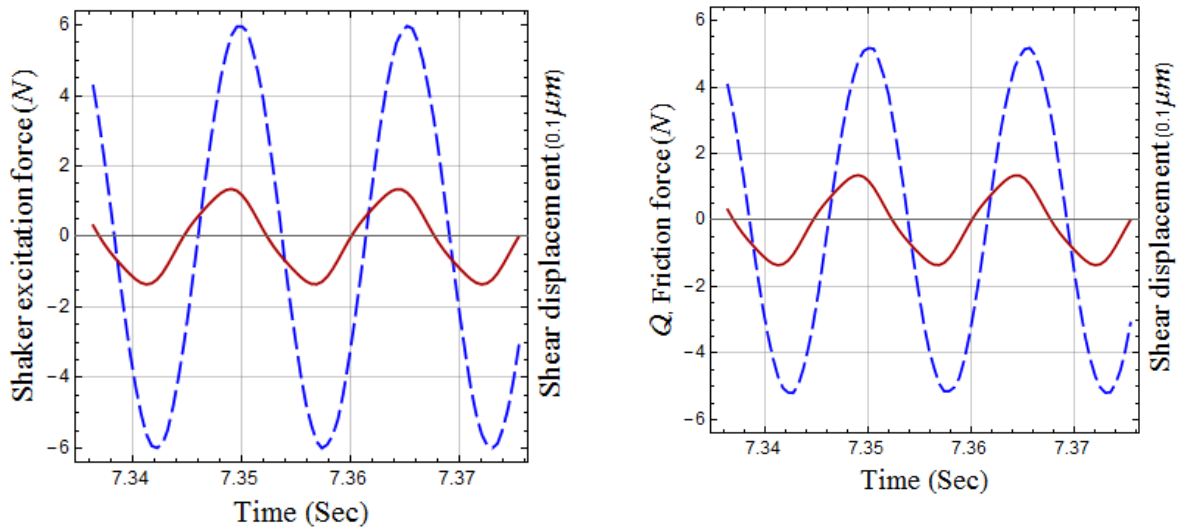

(a) (b)

Fig. 21: Time-domain force (dashed line) and metal block displacement (solid line): (a) Harmonic excitation force at 65 Hz, (b) Resultant friction force.

Also, using the data of Table 2, the proposed equivalent Maxwell slip model of the contact interface is determined. The equivalent Maxwell slip model of the rough interface is produced by L=50 Jenkins elements, using a combination of (N=10 and M=5). Fig. **23** and Fig. **24** compare predicted hysteresis friction force using the equivalent Maxwell slip model and experimentally measured hysteresis friction forces.

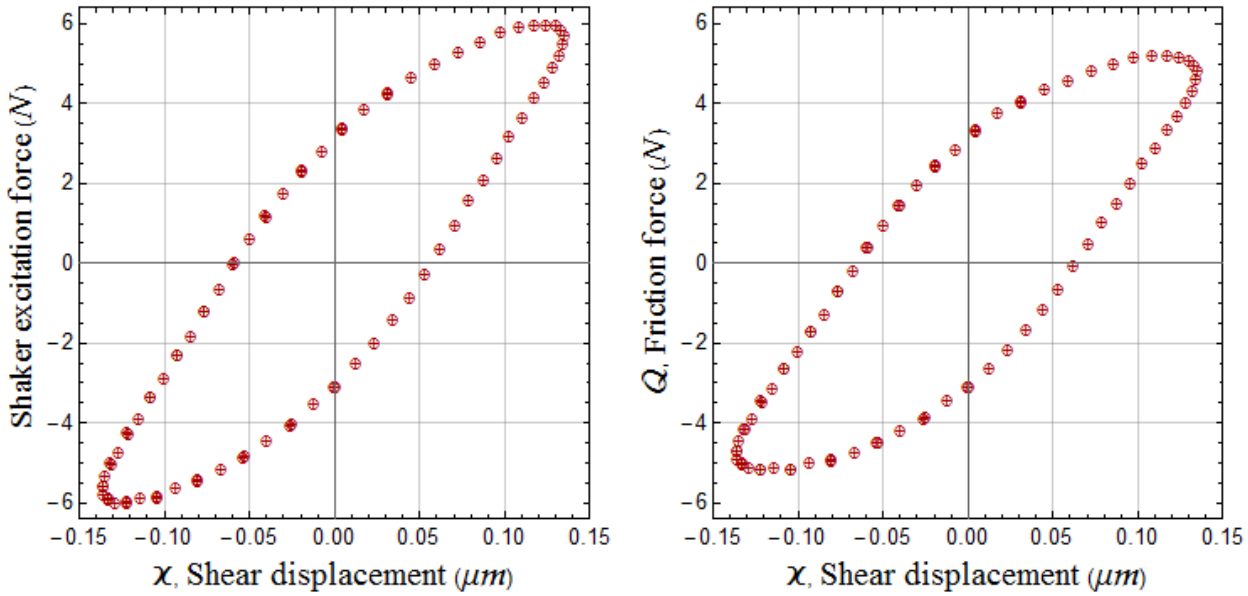

(a) (b)

Fig. 22: Hysteresis loops: (a) Shaker excitation force at 65 Hz vs. shear displacement, (b) Friction force vs. shear displacement.

The frictional hysteresis curves of the rough interface were determined by the proposed multi-asperity contact model of Section 2 using the roughness parameters of Table 2.

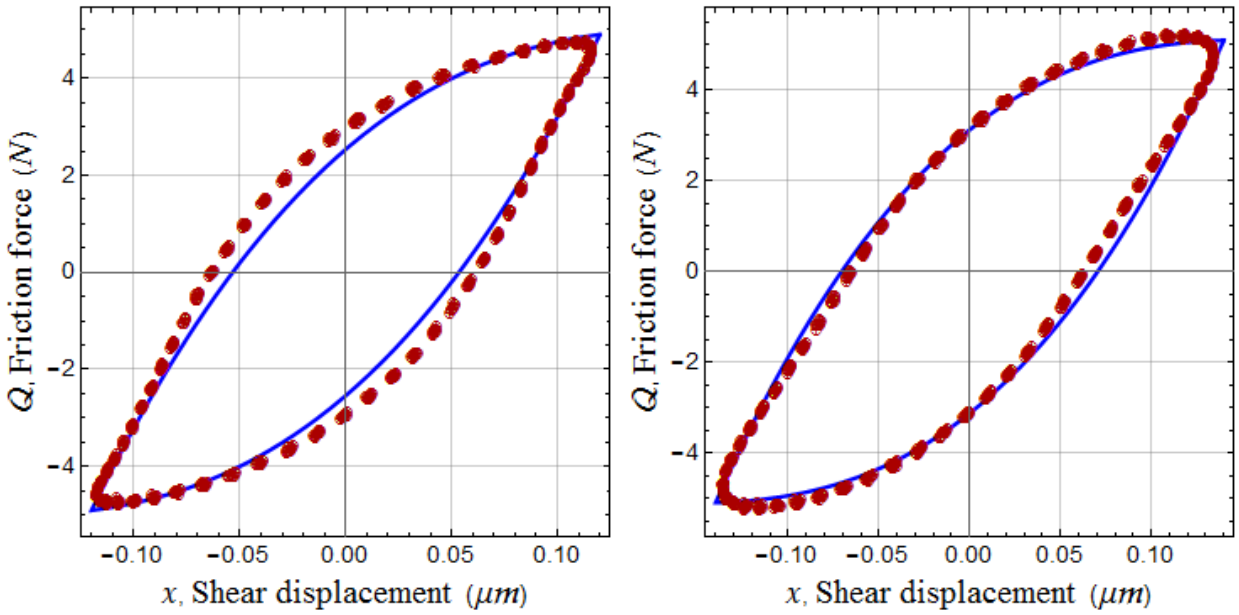

Fig. 23: Hysteresis loops of the proposed Maxwell slip model (solid line) and the test (⊕) at an excitation force of 65 Hz with an amplitude of excitation: (a) 4.5N, (b) 6N.

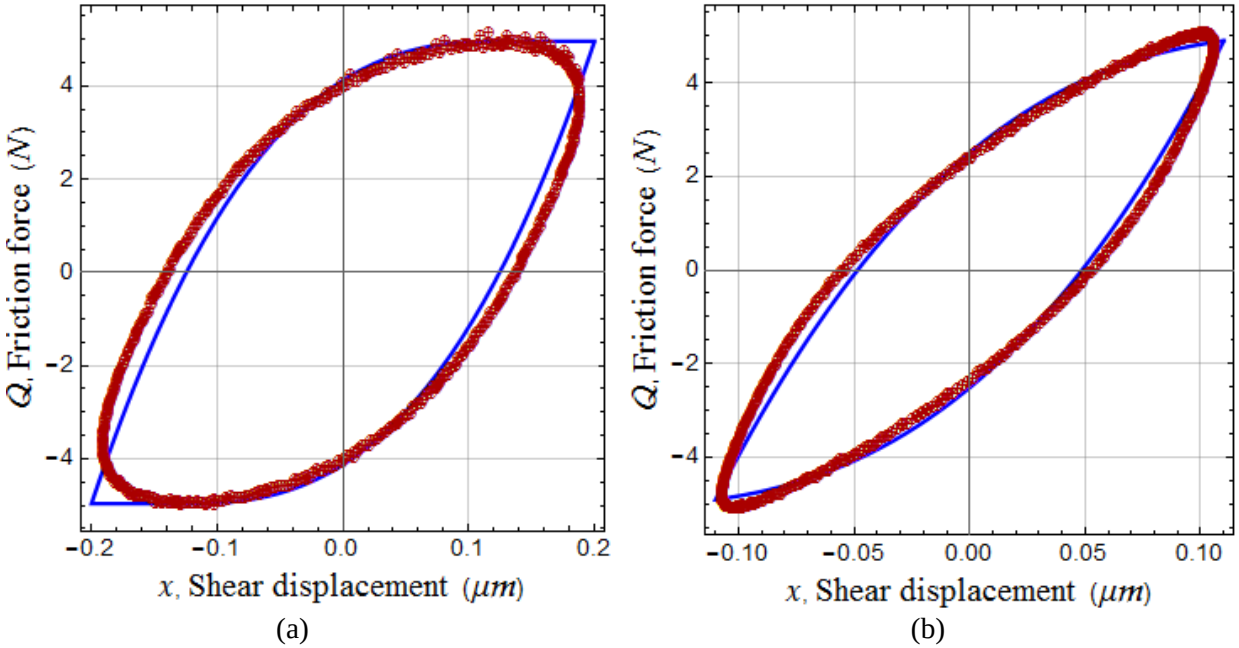

Fig. 24: Hysteresis loops of the proposed Maxwell slip model (solid line) and the test (⊕) at excitation amplitude of 6N: (a) 60Hz, (b) 75Hz.

The resultant curves of Fig. **23** and Fig**. 24** show that the predictions of the hysteresis loop are in good agreement with the test setup's observed behavior. As it is clear in these figures, the frictionally hysteresis curves are slightly affected by rate-dependent damping. The higher amplitude of motion in Fig. **24** (a) is more affected by rate-dependent damping.

It is noted that the experimentally measured hysteresis curves could be simulated by the continuous Iwan model as determined in Section 4, where the predicted hysteresis curves by the Iwan model will be equal to the proposed equivalent Maxwell slip model. As shown in Fig**. 25**(a), the normalized continuous Iwan model of two contacting aluminum blocks is determined using the parameters of Table 2, and its associated hysteresis curve is plotted compared with the experimental result in Fig. **25**(b). The comparison of Fig. **23**(b) and Fig**. 25**(b) shows that the proposed equivalent Maxwell slip model and the determined continuous Iwan model have the same performance in simulating the hysteresis curve.

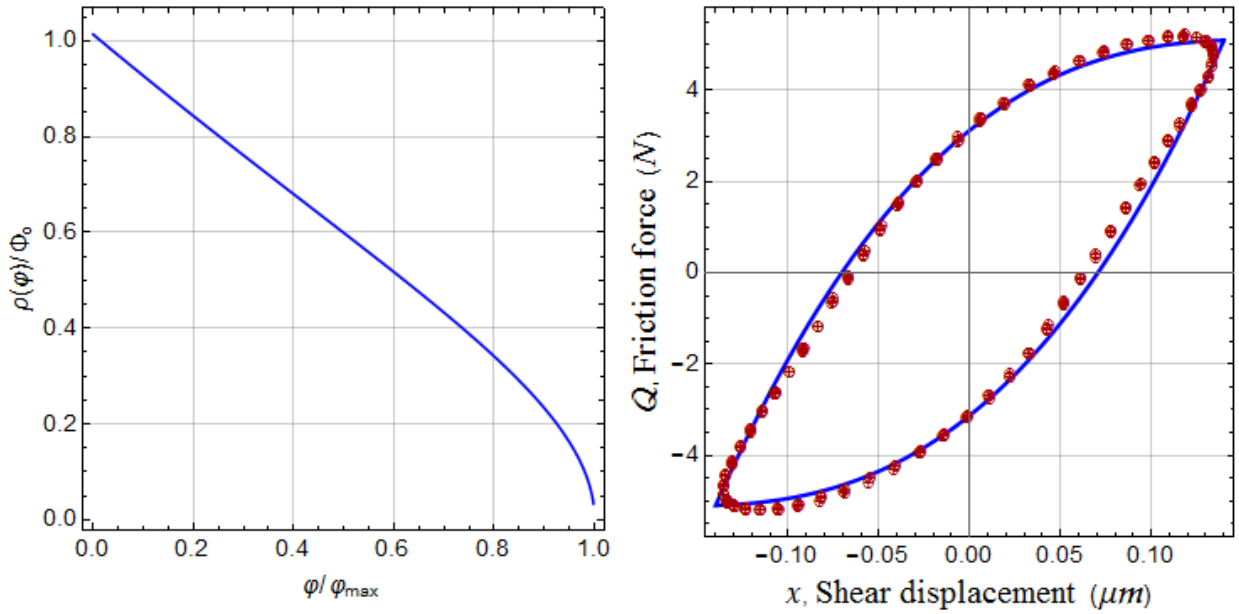

(a) (b)

Fig. 25: The Iwan distribution function and its associated hysteresis loop: (a) The normalized Iwan distribution function of two contacting aluminum blocks, (b) Hysteresis loops due to Iwan function (solid line), and the test (⊕) at excitation force of 65 Hz with an amplitude of excitation 6N.

5.2. Beam with frictional support

The determined continuous Iwan model and the proposed scenario to determine the Maxwell slip model of a rough interface are validated against the experimentally measured behavior of a rough interface. The experimental setup, shown in Fig. **26**, consists of a clamped-frictionally supported steel beam [15, 36, 37].

Fig. 26: Frictionally supported beam test setup [36].

A suspended mass block at frictionally support provides the desired preload, as shown in Fig. **26**. A schematic of the test setup is presented in Fig. **27** to introduce the experimental setup's main features. As shown in this figure, the contacted cylinder flattened for the contact area of the rough interface.

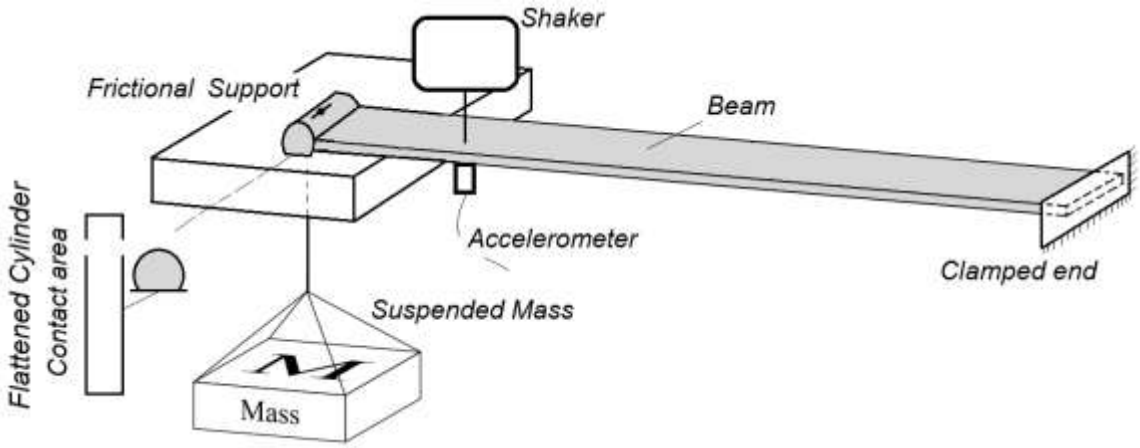

Fig. 27: Schematic of the second test setup.

Roughness characteristics of the contact surfaces were obtained by surface roughness measurements, as reported in Table 3. The surface roughness parameters are calculated using the measured surface topography [40].

Table 3: Material properties and roughness parameters of the identical upper and lower surfaces.

Parameter:	R_{sk}	R_{ku}	R_q	R_{Pc}	R_{sm}
Value:	0.1	3.2	$5.9\mu m$	$51\text{pks}/cm$	$300\mu m$
Parameter:	E_i	ν_i	A	S/H	
Value:	$200Gpa$	0.3	$100mm^2$	0.35	

The structure's dynamic responses were measured while the contact surface was loaded with a 15kg mass block. The block provided a preload of 147 N. A single harmonic excitation was applied to the beam with different amplitudes, resulting in 2g, 3g, 4g, and 5g acceleration levels at the excitation point, generating pre-slip and macro-slip regimes in the contact. These excitations were designated with the resultant direct point zero-pick accelerations; the vertical force variation produced with 15kg of the mass block is negligible at low acceleration levels. The friction force and displacement are calculated considering the Euler-Bernoulli beam, shaker excitation force, and acceleration response, but it is not measured directly [36]. Using the contact data in Table 3, the normalized slippage distribution function of the continuous Iwan model is determined according to Fig**. 28**, and then the hysteresis friction behavior of the rough interface is predicted.

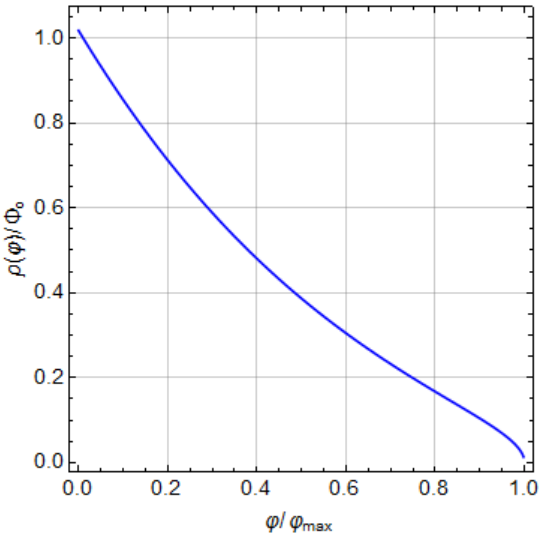

Fig. 28: Normalized Iwan distribution function of frictional support.

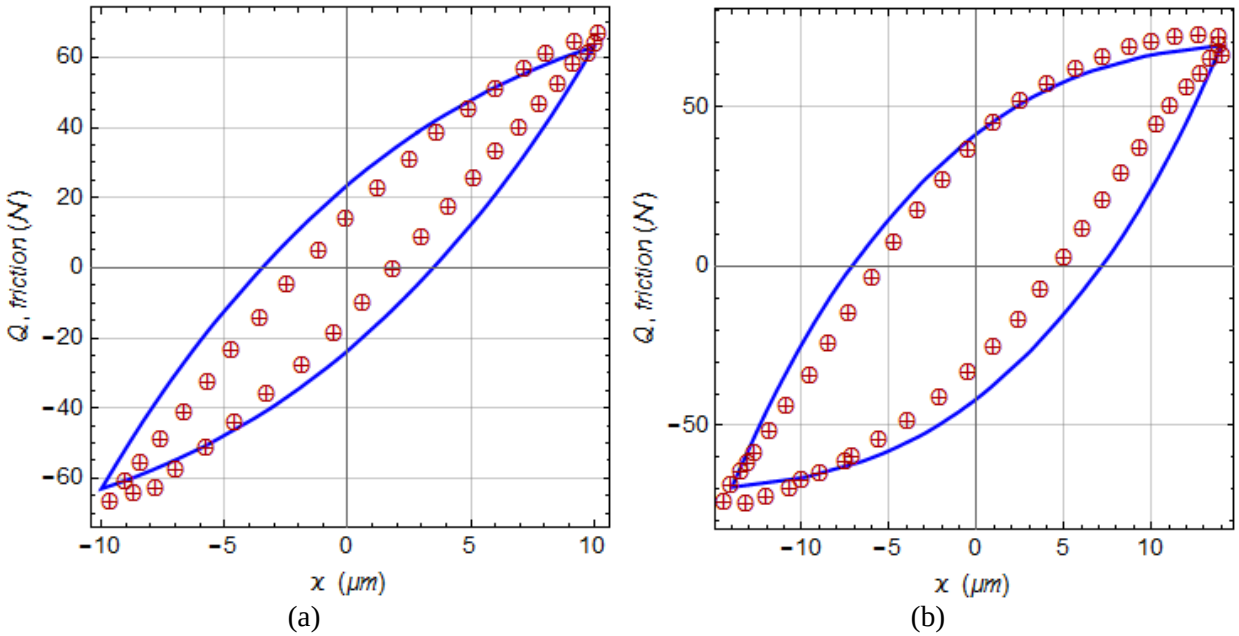

(a) (b)

Fig. 29: Resultant hysteresis loops predicted by continuous Iwan model (solid line), and the test (⊕) [37]; direct point accelerations: (a) 2g, (b)3g.

Fig. **29** and Fig. **30** show the hysteresis curves at pre-slip and macro-slip states, respectively. As shown in Fig. **29** and Fig. **30**, the simulated hysteresis curves by the continuous Iwan model agree with the test results.

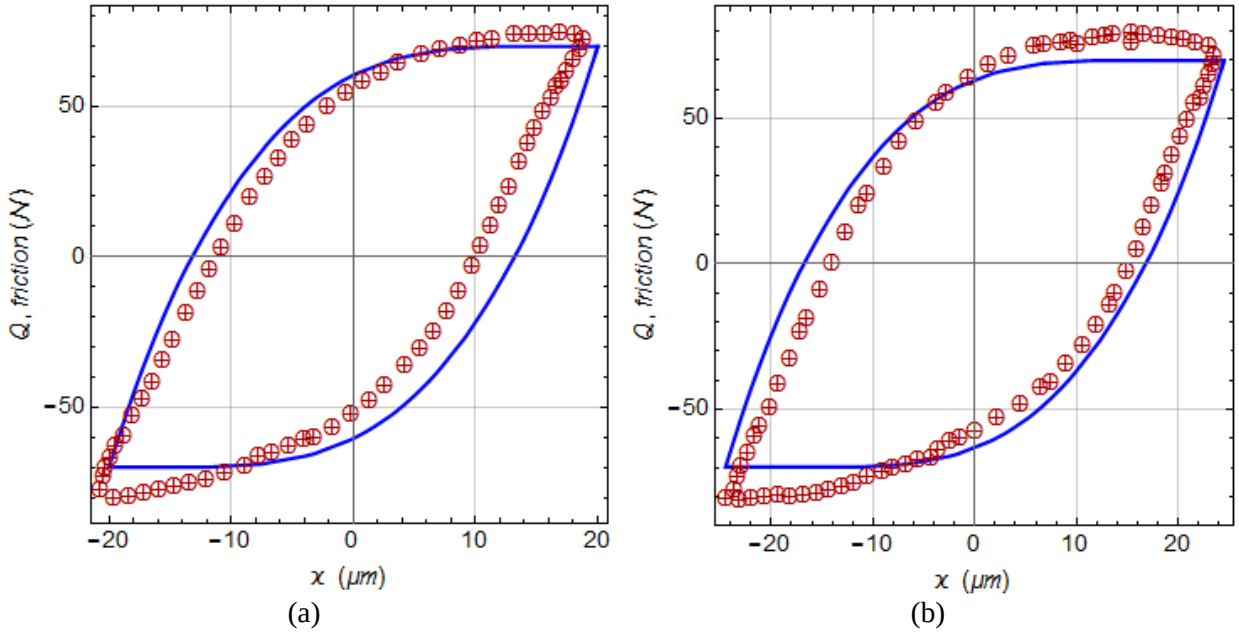

Fig. 30: Resultant hysteresis loops predicted by continuous Iwan model (solid line) and the test (⊕) [37]; direct point accelerations: (a) 4g, (b)5g.

The resultant hysteresis curves of Fig. **29** and Fig. **30** show that the proposed model can be employed to simulate the rough interface frictional behavior using the continuous Iwan model, which is in agreement with the test results. In these figures, the test results do not precisely match the simulation results, which can be due to the following reasons. In the test setup, the normal contact force is not constant, where the tip of the beam as a contact interface vibrates in the normal direction. Hence, the normal force is not completely constant and changes slightly, which does not align with the model assumptions. In the condition of variable normal load, the hysteresis friction curves will be asymmetric [22]. As it is clear from Fig. **30**, the measured hysteresis curves are asymmetric and affected by the variation of normal contact load. Although the variation of normal contact force is lower than 8%, the preload can be considered almost constant. In the first test specimen (Fig. **20**), the weight of the aluminum block mass provides the normal contact force, and there is no excitation or vibration in the normal direction. Therefore, the normal contact force in the first test is completely static and constant. Thus, it does not cause a mismatch in the test and model validation. In the second test, the inertial of the suspended blocks is imported and causes a variable normal contact force phenomenon. Because the model presented in this paper shows that the normal force is modeled as constant and static, this phenomenon caused more discrepancies between the results of the second test and the model concerning the first test.

On the other hand, in the first test, the resulting hysteresis curve is strongly affected by rate-dependent damping due to the use of an almost linear spring. In contrast, in the second test, this phenomenon is not observed clearly, and the test results are only affected by the slight structural damping caused by the vibrating beam. In addition, the multi-asperity contact model is based on

statistical summation. Therefore, with the larger interface area, the simulation results will be more consistent with the test results. This is why the contact area in the second test specimen is much smaller than the first specimen, so the mismatch between the model and the results is increased.

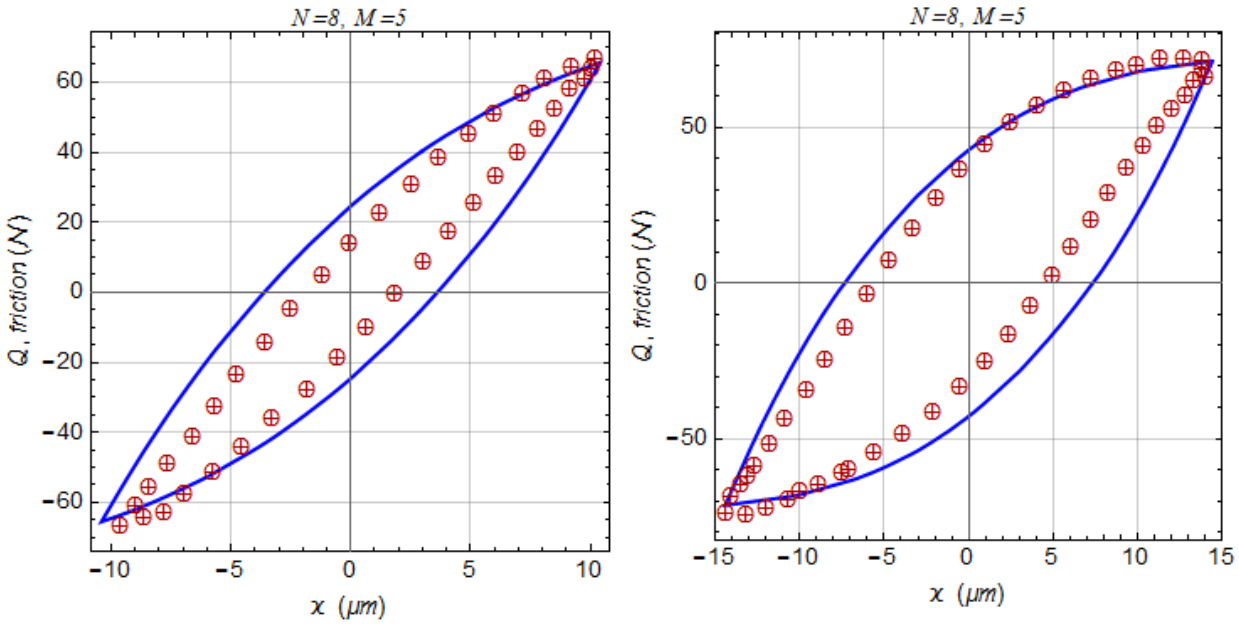

(a) (b)

Fig. 31: Resultant hysteresis loops predicted by Maxwell slip model (solid line), and the test (⊕) [37]; direct point accelerations: (a) 2g, (b)3g.

By contact data of Table 3, the hysteresis friction curves of frictional support are determined using L=40 Jenkins elements of the proposed Maxwell slip model (N=8, M=5) compared with test data according to Fig. **31**. The comparison of Fig. **29** and Fig. **31** shows that the Maxwell slip model has the same results as the continuous Iwan model.

6. Conclusion

This paper introduces a procedure to simulate the behavior of frictional elastic rough interfaces. An equivalent Maxwell slip model, composed of a parallel series of Jenkins elements, is determined analytically using contact surfaces' roughness parameters and material properties. The Jenkins element stiffness and slippage friction force are determined using a single rough interface contact model defined by the classical Mindlin solution and the Hertzian law of spherical asperities contact. The Jenkins elements' characteristics are defined based on their associated heights region of contacting asperities and the state of motion on the asperity scale. Using a few Jenkins elements, the proposed scenario produces accurate predictions of the frictional interface hysteresis behavior. Also, using the multi-asperity contact theory, the slippage force distribution function of the continuous Iwan model was obtained. It is shown that the Maxwell slip model's performance with enough Jenkins elements and the continuous Iwan model is the same, and these two models can be used interchangeably. Numerical and experimental studies show that the proposed process to determine the rough interface's Maxwell slip model accurately simulates the frictional hysteresis behavior of rough interfaces.

Appendix A

The calculation process of the proposed Maxwell slip model of the rough interface is summarized in the following steps:

Step 1: Specifying material properties $E, \nu,$ A , rough surface parameters $\sigma, \bar{R}, \eta$, and friction coefficient model μ .

Step 2: Calculating the distance of the reference plane of two surfaces y , concerning normal interface load F_{υ} , using Equation (27).

Step 3: Select the number of asperities height-region N to establish the vector $\vec{\mathbf{Z}}$ in Equation (40) and calculate the number of asperities involved between z_{n-1} and z_n , using Equation (41). In addition to *N*'s value, the total number of Jenkins elements ($N \times M$) affects the smoothness and accuracy of hysteresis friction curves.

Step 4: Calculate the mean radius of the contact area for each height region, i.e., in the region between z_{n-1} and z_n , using Equation (46).

Step 5: Calculating the normal contact force for each height region of asperities within the range of z_{n-1} , and z_n , using Equation (42).

Step 6: Determination of normal pressure distribution on the mean radius of the contact area $\bar{a}_n$ of Step 4 due to the normal contact force $F_{\upsilon,n}$ of Step 5, using Equation (48).

Step 7: Calculating the initial tangential stiffness of asperities for each height region, within the range of z_{n-1} , and z_n , using Equation (55).

Step 8: Selection of the number of asperities annulus elements M to establish the vector $\vec{\boldsymbol{\rho}}$, according to Equation (50). In the particular case of identical width of annular areal elements, it is,

$$\Delta r_{m,n} = \frac{\bar{a}_n}{M}, \quad r_{m,n} = m\,\Delta r_{m,n}, \quad m = 0,1,...,M, \quad n = 1,2,...,N. \tag{A- 1}$$

Step 9: Calculate the equivalent normal force of each areal element using Equation (49).

Step 10: Calculate each Jenkins element of the Maxwell slip model's slippage friction force using Equation (51).

Step 11: Calculate the stiffness of each Jenkins element of the Maxwell slip model using Equation (57). By Considering Step 8, the Jenkins element stiffness can be obtained as:

$$K_{\tau,n,m} = \frac{K_{0,n}}{M}, \quad m = 0,1,...,M, \quad n = 1,2,...,N. \tag{A- 2}$$

Appendix B

Alternatively, the distribution function of asperity heights can be defined by the relative approach of contacting surfaces, such as Demkin's law [30]. In this case, the tangential friction force of two contacting rough surfaces in the virgin loading phase of Equation (28) can be written as [30]:

$$Q_v(x) = \mu F_\upsilon - \mu \overline{z}_{\max}{}^{3/2} K\eta \mathrm{A} \int_0^{\tilde{\xi}} (\tilde{\xi} - \xi)^{3/2} \Psi'(\xi)\, d\xi,$$
$$\tilde{\xi} = \varepsilon - \frac{x}{\lambda \overline{z}_{\max}}. \tag{B- 1}$$

Where ε is the relative approach of contacting surfaces and Ψ' is derivative of asperity heights distribution function to the relative approach [30]. By substitution of Equation (B- 1) into Equation (64), the slippage distribution function of the Iwan model is obtained as follows:

$$\rho(\varphi) = \frac{3\mu}{4\lambda^2 \overline{z}_{\max}{}^{1/2}} K\eta \mathrm{A} \int_0^{\bar{\xi}} (\bar{\xi} - \xi)^{-1/2}\, \Psi'(\xi)\, d\xi,$$
$$\bar{\xi} = \tilde{\xi}\big|_{x=\varphi}. \tag{B- 2}$$

The normal approach of contacting surfaces d is equal to [30]:

$$d = \varepsilon \overline{z}_{\max}. \tag{B- 3}$$

Also, using the upper bound of asperity height and distance of contacting surfaces, the normal approach can be written as:

$$d = \overline{z}_{\max} - y. \tag{B- 4}$$

Considering Equations (B- 3) and (B- 4), it can be written:

$$y = \overline{z}_{\max}(1 - \varepsilon). \tag{B- 5}$$

Concerning the asperity height distribution function $\Psi(\varepsilon)$, the number of contacting asperities of the rough interface can be obtained as [30]:

$$n_a = \eta \mathrm{A} \int_0^{\varepsilon} \Psi'(\xi)\, d\xi, \quad \Psi'(\varepsilon) = \frac{\partial \Psi(\varepsilon)}{\partial \varepsilon}. \tag{B- 6}$$

By comparison of Equation (B- 6) and Equation (25), it can be deduced,

$$\int_y^{\overline{z}_{\max}} \Phi(z)\, dz = \Psi(\varepsilon). \tag{B- 7}$$

Concerning Equations (B- 7) and (B- 5), the variation of the asperity heights distribution function to the relative approach ε, can be written as:

$$\Psi'(\varepsilon) = -\frac{\partial y}{\partial \varepsilon} \Phi(y) = \overline{z}_{\max} \Phi(\overline{z}_{\max}(1 - \varepsilon)). \tag{B- 8}$$

or,

$$\Psi'(\xi) = \overline{z}_{\max}\Phi(\overline{z}_{\max}(1-\xi)). \tag{B- 9}$$

By substitution of Equation (B- 9) into Equation (B- 2) and considering variable change as:

$$z = \overline{z}_{\max}(1-\xi), \tag{B- 10}$$

it can be written,

$$\rho(\varphi) = \frac{3\mu}{4\lambda^2} K\eta A \int_{y+\frac{\varphi}{\lambda}}^{\overline{z}_{\max}} (z - y - \frac{\varphi}{\lambda})^{-1/2}\Phi(z)\,dz. \tag{B- 11}$$

Concerning Equation (23), it is clear that Equation (B- 11) agrees with Equation (66).

Reference

[1] D.J. Segalman, An initial overview of Iwan modeling for mechanical joints, in, Sandia National Labs., Albuquerque, NM (US); Sandia National Labs …, 2001.

[2] H. Olsson, K.J. Åström, C.C. De Wit, M. Gäfvert, P. Lischinsky, Friction models and friction compensation, European journal of control, 4 (1998) 176-195.

[3] B.D. Nguyen, Modelling of frictional contact conditions in structures, Georgia Institute of Technology. MSc. thesis, (2005).

[4] W.D. Iwan, A distributed-element model for hysteresis and its steady-state dynamic response, Journal of Applied Mechanics, 33 (1966) 893-900.

[5] D.J. Segalman, A four-parameter Iwan model for lap-type joints, Journal of Applied Mechanics, 72 (2005) 752-760.

[6] F. Al-Bender, K. De Moerlooze, On the relationship between normal load and friction force in pre-sliding frictional contacts. Part 1: Theoretical analysis, Wear, 269 (2010) 174-182.

[7] M. Ruderman, T. Bertram, Two-state dynamic friction model with elasto-plasticity, Mechanical Systems and Signal Processing, 39 (2013) 316-332.

[8] H. Ahmadian, M. Rajaei, Identification of Iwan distribution density function in frictional contacts, Journal of Sound and Vibration, 333 (2014) 3382-3393.

[9] K. Worden, C. Wong, U. Parlitz, A. Hornstein, D. Engster, T. Tjahjowidodo, F. Al-Bender, D. Rizos, S. Fassois, Identification of pre-sliding and sliding friction dynamics: Grey box and black-box models, Mechanical systems and signal Processing, 21 (2007) 514-534.

[10] T. Tjahjowidodo, Theoretical analysis of the dynamic behavior of presliding rolling friction via skeleton technique, Mechanical Systems and Signal Processing, 29 (2012) 296-309.

[11] S. Kang, H. Yan, L. Dong, C. Li, Finite-time adaptive sliding mode force control for electro-hydraulic load simulator based on improved GMS friction model, Mechanical Systems and Signal Processing, 102 (2018) 117-138.

[12] G. Aguirre, T. Janssens, H. Van Brussel, F. Al-Bender, Asymmetric-hysteresis compensation in piezoelectric actuators, Mechanical Systems and Signal Processing, 30 (2012) 218-231.

[13] P.-P. Yuan, W.-X. Ren, J. Zhang, Dynamic tests and model updating of nonlinear beam structures with bolted joints, Mechanical Systems and Signal Processing, 126 (2019) 193-210.

[14] N.N. Balaji, M.R. Brake, The surrogate system hypothesis for joint mechanics, Mechanical Systems and Signal Processing, 126 (2019) 42-64.

[15] H. Ahmadian, M. Mohammadali, A distributed mechanical joint contact model with slip/slap coupling effects, Mechanical Systems and Signal Processing, 80 (2016) 206-223.

[16] S. Bograd, P. Reuss, A. Schmidt, L. Gaul, M. Mayer, Modeling the dynamics of mechanical joints, Mechanical Systems and Signal Processing, 25 (2011) 2801-2826.

[17] J. Greenwood, J. Tripp, The contact of two nominally flat rough surfaces, Proceedings of the institution of mechanical engineers, 185 (1970) 625-633.

[18] J.A. Greenwood, J.B.P. Williamson, Contact of nominally flat surfaces, Proceedings of the Royal Society of London A: Mathematical, Physical and Engineering Sciences, 295 (1966) 300-319.

[19] M. Eriten, A.A. Polycarpou, L.A. Bergman, Physics-based modeling for fretting behavior of nominally flat rough surfaces, International Journal of Solids and Structures, 48 (2011) 1436-1450.

[20] A. Majumdar, B. Bhushan, Fractal model of elastic-plastic contact between rough surfaces, Journal of Tribology, 113 (1991) 1-11.

[21] J. Greenwood, J. Wu, Surface roughness and contact: an apology, Meccanica, 36 (2001) 617-630.

[22] H. Jamshidi, H. Ahmadian, A Modified rough interface model considering shear and normal elastic deformation couplings, International Journal of Solids and Structures, 203 (2020) 57-72.

[23] K.L. Johnson, Contact mechanics, Cambridge university press, 1987.

[24] P.R. Nayak, Random process model of rough surfaces, Journal of Lubrication Technology, 93 (1971) 398-407.

[25] C. Cattaneo, Sul contatto di due corpi elasticie: Distribution locale degli sforzi, Reconditi dell Academia Nazionale die Lincei, 27 (1938) 474-478.

[26] R.D. Mindlin, Compliance of elastic bodies in contact, Journal of Applied Mechanics, 16 (2021) 259-268.

[27] Y.F. Gao, B.N. Lucas, J.C. Hay, W.C. Oliver, G.M. Pharr, Nanoscale incipient asperity sliding and interface micro-slip assessed by the measurement of tangential contact stiffness, Scripta Materialia, 55 (2006) 653-656.

[28] W. Zhan, P. Huang, Modeling tangential contact based on non-Gaussian rough surfaces, Proceedings of the Institution of Mechanical Engineers, Part J: Journal of Engineering Tribology, 233 (2018) 51-60.

[29] N. Yu, A.A. Polycarpou, Contact of rough surfaces with asymmetric distribution of asperity heights, J. Trib., 124 (2002) 367-376.

[30] I.I. Argatov, E.A. Butcher, On the Iwan models for lap-type bolted joints, International Journal of Non-Linear Mechanics, 46 (2011) 347-356.

[31] N. Yu , A.A. Polycarpou, Combining and contacting of two rough surfaces with asymmetric distribution of asperity heights, Journal of Tribology, 126 (2004) 225-232.

[32] W. Zhan, P. Huang, Modeling tangential contact based on non-Gaussian rough surfaces, Proceedings of the Institution of Mechanical Engineers, Part J: Journal of Engineering Tribology, 233 (2019) 51-60.

[33] D. Wang, C. Xu, X. Fan, Q. Wan, Reduced-order modeling approach for frictional stick-slip behaviors of joint interface, Mechanical Systems and Signal Processing, 103 (2018) 131-138.

[34] M. Ruderman, T. Bertram, Modified Maxwell-slip model of presliding friction, IFAC Proceedings Volumes, 44 (2011) 10764-10769.

[35] J. Chen, J. Zhang, J. Hong, L. Zhu, Modeling tangential contact of lap joints considering surface topography based on Iwan model, Tribology International, 137 (2019) 66-75.

[36] M. Rajaei, H. Ahmadian, Development of generalized Iwan model to simulate frictional contacts with variable normal loads, Applied Mathematical Modelling, 38 (2014) 4006-4018.

[37] H. Ahmadian, H. Jalali, F. Pourahmadian, Nonlinear model identification of a frictional contact support, Mechanical Systems and Signal Processing, 24 (2010) 2844-2854.

[38] H. Jamshidi, A. Koochakinejad, Analytical determination of Bouc-Wen friction model of Two contacted flat rough surfaces in elastic region, Journal of Theoretical and Applied Vibration and Acoustics, 7 (2021) -.

[39] A. Mahmoodi, H. Ahmadian, Coupling between the tangential and normal direction in turbine blade forced vibration analysis, Journal of Vibration Engineering & Technologies, (2022) 1-11.

[40] J.I. McCool, Comparison of models for the contact of rough surfaces, Wear, 107 (1986) 37-60.